Vapor-phase chemical equilibrium and combined chemical and vapor-liquid equilibrium for the ternary system ethylene + water + ethanol from reaction-ensemble and reactive Gibbs-ensemble molecular simulations

Y. Mauricio Muñoz-Muñoz [a,b], Jadran Vrabec[b], Mario Llano-Restrepo [a]*

[a] School of Chemical Engineering, Universidad del Valle,
Ciudad Universitaria Melendez, Building 336,
Apartado 25360, Cali, Colombia

[b] Thermodynamics and Energy Technology,
University of Paderborn, 33098 Paderborn, Germany

* Corresponding author. Tel: + 57-2-3312935; fax: + 57-2-3392335
E-mail address: mario.llano@correounivalle.edu.co (M. Llano-Restrepo)

Abstract

Reliable combined chemical and vapor-liquid equilibrium (ChVLE) data for the ternary system ethylene + water + ethanol are required for the conceptual design of a reactive separation process to obtain ethanol by the hydration of ethylene. Due to the absence of experimental data for the combined ChVLE of the reacting system, molecular simulation looks appealing to predict such data. In this work, the reaction-ensemble Monte Carlo (RxMC) method was used to calculate the chemical equilibrium of the ternary system in the vapor phase, and the reactive Gibbs-ensemble Monte Carlo (RxGEMC) method was used to calculate its combined ChVLE. A set of previously validated Lennard-Jones plus point-charge potential models were employed for ethylene, water, and ethanol. The RxMC predictions for the vapor-phase chemical equilibrium composition of the ternary system and the equilibrium conversion of ethylene to ethanol, at 200°C and pressures of 30, 40, 50, and 60 atm, were found to be in good agreement with predictions made by use of a previously proposed thermodynamic model that combines the Peng-Robinson-Stryjek-Vera equation of state, the Wong-Sandler mixing rules, and the UNIQUAC activity coefficient model. The RxGEMC calculations were used to predict the reactive phase diagram (two-dimensional graph of pressure versus transformed liquid and vapor-phase ethylene mole fractions) at 200°C. In contrast to the thermodynamic model, molecular simulation predicts a wider reactive phase diagram (due to a reactive dew-point line much richer in ethylene). However, these two independent approaches were found to be in very good agreement with regard to the predicted bubble-point line of the reactive phase diagram and the approximate location of the reactive critical point.

Keywords: Chemical equilibrium; reactive phase equilibrium; ternary systems; reactive critical point; ethylene hydration; petrochemical ethanol.

1. Introduction

The concept of process intensification could be applied in the petrochemical industry to the production of ethanol by the direct hydration of ethylene. In the intensified process, the simultaneous reaction and separation of the product (ethanol) and the reactants (ethylene and water) would occur in the same piece of equipment, a reactive separation column, into which gaseous ethylene and liquid water would be fed [1].

In a previous study [2], we corroborated the validity of a set of previously published Lennard-Jones plus point-charge potential models for ethylene [3], water [4], and ethanol [5] from the good agreement of Gibbs-ensemble Monte Carlo (GEMC) molecular simulation results for the vapor pressure and the VLE phase diagrams of those components with respect to calculations made by means of the most accurate (reference) multiparameter equations of state currently available for ethylene [6], water [7], and ethanol [8]. We found that these potential models are capable of predicting the available VLE phase diagrams of the binary systems ethylene + water [9] (at 200 and 250°C), ethylene + ethanol [10] (at 150, 170, 190, 200, and 220°C), and ethanol + water [11] (at 200, 250, 275, and 300°C). We also found that molecular simulation predictions for the VLE phase diagrams of the ternary system ethylene + water + ethanol, at 200°C and pressures of 30, 40, 50, 60, 80, and 100 atm, are in very good agreement with both the experimental data [12] and predictions that we had previously made [1] by use of a thermodynamic model that combines the Peng-Robinson-Stryjek-Vera (PRSV2) equation of state [13, 14], the Wong-Sandler (WS) mixing rules [15], and the UNIQUAC activity coefficient model [16]. This agreement between the predictions of two independent methods (molecular simulation and the thermodynamic model) gave us confidence for the subsequent use of simulation to predict the combined chemical and vapor-liquid equilibrium (ChVLE) of the ternary system and check the validity of predictions that we previously made [1] by means of the thermodynamic model.

The reaction-ensemble Monte Carlo (RxMC) method [17-19] has been used successfully by several authors for the computation of the chemical equilibrium of some reactions of industrial

interest, such as the dimerization of nitric oxide [20-22], the esterification reaction of ethanol and acetic acid to yield ethyl acetate and water [23], the hydrogenation of benzene to cyclohexane [24], the synthesis of ammonia [20, 25, 26], and the combined hydrogenation of ethylene and propylene [27]. A very comprehensive review of the RxMC method and its various applications has been made by Turner et al. [19]. In this work, the RxMC method was implemented in order to compute the vapor-phase chemical equilibrium of the ternary system ethylene + water + ethanol (i.e., for the vapor-phase hydration of ethylene to ethanol) and compare the simulation predictions with those obtained by means of the PRSV2-WS-UNIQUAC thermodynamic model described in the first of our previous works [1].

The reactive Gibbs-ensemble Monte Carlo (RxGEMC) method [18, 28, 29] is a combination of the reaction-ensemble (RxMC) [17-19] and the Gibbs-ensemble (GEMC) [30-37] methods, and it has already been used for the computation of the combined ChVLE of dimerization and combination reactions [18, 28] and the etherification reaction of isobutene and methanol to produce methyl-tert-butyl ether [29]. In this work, the RxGEMC method was implemented in order to compute the combined ChVLE for the hydration of ethylene to ethanol and compare the simulation predictions with those previously obtained [1] from the thermodynamic model.

The outline of the paper is as follows. The RxMC and the RxGEMC simulation methods are described in Sections 2.1 and 2.2, respectively. In Section 3.1, simulation results for the vapor-phase chemical equilibrium of the hydration reaction are reported, discussed, and compared with calculations previously carried out [1] by means of the PRSV2-WS-UNIQUAC thermodynamic model. In Section 3.2, simulation results for the combined ChVLE of the hydration reaction are reported, discussed, and compared with the predictions previously made [1] by use of the thermodynamic model.

2. Simulation methods

The Lennard-Jones (LJ) plus point-charge intermolecular potential models recently devised by Weitz and Potoff [3] for ethylene, Huang et al. [4] for water, and Schnabel et al. [5] for ethanol

were used to carry out the simulations of the present work. These potential models were described in detail in our previous simulation study [2], and their validity was corroborated from the good agreement obtained between our simulation results for the vapor pressure and the VLE phase diagrams of those pure components [2] and calculations carried out by means of the most accurate (reference) multiparameter equations of state currently available [6-8]. For all simulations carried out in the present work, the Lorentz-Berthelot combining rules were used to calculate the size and energy parameters of the LJ potential for unlike interactions [2].

2.1 Simulation method for the vapor-phase chemical equilibrium

In the reaction-ensemble Monte Carlo (RxMC) method, a single simulation box is used to simulate the vapor-phase chemical equilibrium of a reversible reaction like the hydration of ethylene to ethanol:

$$C_2H_4 + H_2O \leftrightarrow C_2H_5OH$$

There are three types of random moves for the RxMC method [17-19] when dealing with rigid molecules: translational displacement and rotation of molecules inside the simulation box, box volume changes, and reaction steps. The moves are accepted or rejected in accordance with a particular probability recipe that involves the calculation of the total intermolecular potential energy change $\Delta U_t = U_t^n - U_t^o$ between the new (U_t^n) and the old (U_t^o) configurations. The molecular displacements and rotations, and the box volume changes are carried out in the same way as in the *NPT*-ensemble, with the usual probability formulas for the acceptance or rejection of those trial moves [38, 39]. For the rotational moves required for water and ethanol, the orientational displacements followed the scheme [38] that chooses random values for the Euler angles in the rotation matrix, and employs the internal coordinates of the sites of the molecule [2] to calculate their simulation-box coordinates. The probability of acceptance for the reaction steps is given by the expression [17, 19]:

$$P_{rx} = \min\left\{1, \left(\frac{P^0 V}{k_B T}\right)^{\bar{\nu}\zeta} (K_{eq})^{\zeta} \exp\left(-\frac{\Delta U_t}{k_B T}\right) \prod_{i=1}^{C}\left[\frac{N_i!}{(N_i + \nu_i \zeta)!}\right]\right\} \quad (1)$$

where P^0 is the standard-state pressure, V is the volume of the simulation box, k_B is the Boltzmann constant, T is the absolute temperature, K_{eq} is the chemical equilibrium constant of the reaction, C is the number of components in the reacting system, $\bar{\nu} = \sum_{i=1}^{C} \nu_i$ with ν_i as the stoichiometric coefficient of component i (positive for products and negative for reactants), $\zeta = +1$ for the reaction in the forward direction, $\zeta = -1$ for the reaction in the backward direction, N_i is the number of molecules of component i before the reaction step is taken, and ΔU_t is the total configurational energy change involved in the reaction step. For the hydration of ethylene to ethanol, the stoichiometric coefficients are $\nu_1 = \nu_2 = -1$ for ethylene (1) and water (2), $\nu_3 = +1$ for ethanol (3), and $\bar{\nu} = -1$ for the reaction.

The chemical equilibrium constant K_{eq} is a function of temperature only. As explained in detail in the first of our previous works [1], K_{eq} is obtained by successively integrating the van't Hoff and Kirchhoff equations (see Eqs. (7) and (8) in Ref. [1]) and making use of a suitable ideal-gas isobaric heat capacity correlation (see Eq. (9) in Ref. [1]). When the standard properties of formation and the coefficients for the heat capacity correlation given in Table 10 of Ref. [1] for ethylene, water, and ethanol are used to carry out the integrations, the following expression for K_{eq} is obtained:

$$K_{eq} = \exp\left(-1.376 \ln T + 2.0785 \times 10^{-3} T - 2.683 \times 10^{-7} T^2 - \frac{6050}{T^2} + \frac{5308.358}{T} - 7.1126\right) \quad (2)$$

In the same way as in our previous work [2], the total intermolecular potential energy U_t was computed as the sum of non-electrostatic and electrostatic contributions. The non-electrostatic

contribution (U_{LJ}) was computed by use of the LJ pair potential model and the electrostatic contribution (U_{Coul}) was computed by means of the Ewald summation method [38-42] for the Coulombic potential, as follows:

$$U_t = U_{LJ} + U_{Coul} = U_{LJ}^{trunc} + U_{LJ}^{corr} + U_{Coul}^{real} + U_{Coul}^{recip} + U_{Coul}^{self} \quad (3)$$

where U_{LJ}^{trunc} is the truncated LJ potential, U_{LJ}^{corr} is the corresponding long-range correction [39, 43], and U_{Coul}^{real}, U_{Coul}^{recip}, and U_{LJ}^{self} are the real space, reciprocal space, and self-interaction terms of the Ewald sum, respectively [38-42]. For all simulations, a spherical cutoff distance $r_c = 8.5$ Å was used to truncate the LJ potential and calculate its long-range correction from the analytical expression given in Refs. [38, 39] and extended to mixtures by de Pablo and Prausnitz [43]. This value for the cutoff distance is a compromise between the values obtained by applying the typical criterion $r_c = 2.5\sigma$ to the LJ contributions to the potential models of ethylene, water, and ethanol (see Table 1 in our previous work [2]). Consistency with the minimum image convention was preserved because the cutoff distance was always less than half the simulation box length. Since the Ewald summation method was used to compute the Coulombic interactions between point charges, then it was not necessary to truncate those interactions and, accordingly, there was no need either for a longer cutoff distance as used in other works in which the Coulombic interactions are calculated by truncation and correction by use of the reaction field method.

As explained in detail in our previous work [2], the time-saving strategy devised by Fartaria et al. [44] was carefully implemented to obtain a significant decrease in the computer time required for the computation of the Ewald sum. Such a strategy consists of using repository matrices to store pairwise potential energies like the truncated LJ potential and the real space term of the Ewald sum, in order to make an efficient calculation of configurational energy changes. In addition to that, a repository matrix was also used to store the complex-variable summation that runs over molecular sites for each reciprocal space vector, in order to make an efficient calculation of changes in the reciprocal space term of the Ewald sum.

To carry out the reaction steps associated to the hydration of ethylene to ethanol, firstly, a direction, forward or backward, to take the reaction step, is randomly chosen. If the forward direction of the reaction is chosen, then an ethylene molecule is randomly selected, and its potential energy of interaction $U_1^{(d)}$ with all the other molecules is calculated before that molecule is deleted from the simulation box. Following this deletion, a water molecule is randomly chosen, and its potential energy of interaction $U_2^{(d)}$ with the remaining molecules is calculated before that molecule is deleted. After this deletion, an ethanol molecule is created (if possible, in the same position as the water molecule that was deleted), and its potential energy of interaction $U_3^{(c)}$ with all the other molecules is calculated. The change of configurational energy for the reaction step in the forward direction is then given by the expression:

$$\Delta U_t^{(f)} = U_3^{(c)} - U_1^{(d)} - U_2^{(d)} \tag{4}$$

By setting $\zeta = +1$, the product in Eq. (1) takes the form:

$$\prod_{i=1}^{C} \frac{N_i!}{(N_i + \nu_i \zeta)!} = \frac{N_1 N_2}{(N_3 + 1)} \tag{5}$$

Substitution of $\overline{\nu} = -1$, $\zeta = +1$, and Eq. (5) into Eq. (1) leads to the following expression for the probability of acceptance of a reaction step in the forward (*f*) direction:

$$P_{rx}^{(f)} = \min\left\{1, \frac{k_B T}{P^0 V} K_{eq} \frac{N_1 N_2}{(N_3 + 1)} \exp\left(-\frac{\Delta U_t^{(f)}}{k_B T}\right)\right\} \tag{6}$$

where the change of configurational energy $\Delta U_t^{(f)}$ is given by Eq. (4).

If the backward direction of the reaction is chosen, then an ethanol molecule is randomly selected, and its potential energy of interaction $U_3^{(d)}$ with all the other molecules is calculated before that molecule is deleted from the simulation box. Following this deletion, a water

molecule is created (if possible, in the same position as the ethanol molecule that was deleted), and its potential energy of interaction $U_2^{(c)}$ with all the other molecules is calculated. Next, an ethylene molecule is created in a random position of the simulation box, and its potential energy of interaction $U_1^{(c)}$ with all the other molecules is calculated. The change of configurational energy for the reaction step in the backward direction is then given by the expression:

$$\Delta U_t^{(b)} = U_1^{(c)} + U_2^{(c)} - U_3^{(d)} \tag{7}$$

By setting $\zeta = -1$, the product in Eq. (1) takes the form:

$$\prod_{i=1}^{C} \frac{N_i!}{(N_i + \nu_i \zeta)!} = \frac{N_3}{(N_1 + 1)(N_2 + 1)} \tag{8}$$

Substitution of $\bar{\nu} = -1$, $\zeta = -1$, and Eq. (8) into Eq. (1) leads to the following expression for the probability of acceptance of a reaction step in the backward (*b*) direction:

$$P_{rx}^{(b)} = \min\left\{1, \frac{P^0 V}{k_B T} \frac{N_3}{K_{eq}(N_1 + 1)(N_2 + 1)} \exp\left(-\frac{\Delta U_t^{(b)}}{k_B T}\right)\right\} \tag{9}$$

where the change of configurational energy $\Delta U_t^{(b)}$ is given by Eq. (7).

For the simulation of the vapor-phase chemical equilibrium of the ternary system at given values of temperature *T* and pressure *P*, the following four-stage strategy was implemented. In the first stage, by specifying the ethylene to water feed mole ratio and defining an initial number of ethanol molecules in the simulation box equal to zero, the initial numbers of ethylene and water molecules were defined from a total number of 400 molecules. In the second stage, an *NVT*-ensemble simulation (with $N = 400$ molecules) was carried out with an arbitrary vapor-density value and for a total number of 1×10^6 moves (molecular displacements and rotations), 60 % of which were used to equilibrate the configurational energy. In the third stage, starting from the

final configuration obtained after the *NVT* run, an *NPT*-ensemble simulation was carried out for a total number of 3×10^6 moves (using a ratio of one volume change to *N* molecular displacements and rotations), 60% of which were used to equilibrate the density and the configurational energy. In the fourth stage, starting from the final configuration obtained after the *NPT* run, a RxMC simulation (at the fixed conditions of temperature *T* and pressure *P*) was carried out for a total number of 1×10^6 moves, using a ratio of 10 volume changes to *N* molecular displacements and rotations and *N* reaction steps, the latter of which were taken in both directions (forward and backward) with equal probability. Ensemble averages were computed for the numbers of molecules of the three components and from these averages, the molar composition of the ternary system in chemical equilibrium was calculated. Statistical uncertainties (error bars) associated to the RxMC ensemble-averages were calculated by means of the block averaging method of Flyvbjerg and Petersen [45].

2.2 Simulation method for the combined chemical and vapor-liquid equilibrium

In the reactive Gibbs-ensemble Monte Carlo (RxGEMC) method [18, 28, 29], two simulation boxes are used to simulate the combined ChVLE equilibrium of a reversible reaction like the hydration of ethylene to ethanol. Besides the three types of random moves already explained in Section 2.1 for the RxMC (i.e., translational displacements and rotations of molecules, box volume changes, and reaction steps in the forward and backward directions), a fourth move type, the transfer of molecules between the boxes (i.e., simultaneous deletion and insertion moves) is performed in order to achieve the phase equilibrium condition of equality of the chemical potentials in the two phases for each component. The probability formulas for the acceptance or rejection of this fourth move type have been discussed in several papers on the GEMC method [30-37] and also in the textbook by Frenkel and Smit [39]. To increase the sampling efficiency, the reaction steps are usually performed in the vapor phase.

For the simulation of the combined ChVLE of the ternary system, the following four-stage strategy was implemented. In the first stage, by specifying the temperature *T* and the pressure *P* of the system, estimates of the molar compositions and densities of the coexisting vapor and

liquid phases at chemical equilibrium were obtained from a reactive *T-P* flash calculation with the help of the PRSV2-WS-UNIQUAC thermodynamic model, as described in detail in the first of our previous works [1]. In the second stage, for each phase of the mixture, an *NVT*-ensemble simulation (with $N = 400$ molecules), with the density and mole fractions fixed at the values estimated from the thermodynamic model, was carried out for a total number of 1×10^7 moves (molecular displacements and rotations), 60% of which were used to equilibrate the configurational energy. In the third stage, starting from the final configuration obtained after the *NVT* runs, an *NPT*-ensemble simulation was carried out for each phase for a total number of 2×10^7 moves (using a ratio of 10 volume changes to *N* molecular displacements and rotations), 60% of which were used to equilibrate the density and the configurational energy. In the fourth stage, starting from the final configurations obtained after the *NPT* runs, a RxGEMC simulation was carried out for the set of two boxes, for a total number of 2×10^7 moves, using a ratio of 10 volume changes for each box to 2*N* molecular displacements and rotations, 2*N* molecular transfers between the boxes, and 2*N* reaction steps in the vapor-phase box, the latter of which were taken in both directions (forward and backward) with equal probability. Properties of the coexisting phases were sampled every 5×10^5 moves, and running averages were recalculated until the statistical equality for the chemical potentials of each component in the two phases was attained. Statistical uncertainties (error bars) associated to the RxGEMC ensemble averages were also calculated by means of the block averaging method of Flyvbjerg and Petersen [45]. In our previous simulation work [2], we found that the VLE phase diagram of ethylene + water at 200°C was improved by the use of a correction factor $\chi = 0.9$ in the Lorentz combining rule $\varepsilon_{i,j} = \chi(\varepsilon_i \varepsilon_j)^{1/2}$ for the energy parameter ε_{ij} of the LJ potential for ethylene-water unlike interactions. That value of the correction factor was also used here to carry out both RxMC and RxGEMC simulations.

3. Simulation results

3.1 Results for the vapor-phase chemical equilibrium

By following the four-stage strategy explained in Section 2.1, RxMC simulations of the vapor-phase chemical equilibrium for the ternary system ethylene + water + ethanol were carried out at a temperature of 200°C and pressures of 30, 40, 50, and 60 atm. Simulations were started by specifying values of the ethylene to water feed mole ratio such that the initial ethylene mole fraction in the simulation box was in the range from 0.1 to 0.9.

The computed chemical equilibrium molar composition diagrams are shown in Figs. 1-4, where the filled circles correspond to the molecular simulation results, and both the empty circles and the solid line correspond to the results obtained by means of the PRSV2-WS-UNIQUAC thermodynamic model [1]. The dotted lines are used to join the initial (feed) compositions, marked by the empty squares, and the final (equilibrium) compositions of the ternary system. As indicated by the longest dotted line in these diagrams, the possible maximum value of the equilibrium mole fraction of ethanol would correspond to an initial equimolar ethylene + water mixture, and this maximum mole fraction increases with pressure.

The computed values of the equilibrium conversion of ethylene to ethanol as a funtion of the ethylene to water feed mole ratio are shown in Figs. 5-8, where the filled circles correspond to the molecular simulation results, the solid line corresponds to the results obtained from the thermodynamic model (i.e., for the non-ideal gas mixture), and the empty squares correspond to the assumption of ideal-gas behavior. As follows from Figs. 5-8, at all pressures, the equilibrium conversion of ethylene to ethanol decreases with increasing values of the ethylene to water feed mole ratio. Also, for a given value of the ethylene to water feed mole ratio, the equilibrium conversion increases with increasing pressure. Simulation predictions for the equilibrium conversion are in fairly close agreement with the predictions made by use of the thermodynamic model. The minimum deviation between the simulation predictions and the results from the thermodynamic model is 1.7% at 30 atm, 1.6% at 40 atm, 2.9% at 50 atm, and 0.6% at 60 atm. In contrast, results for the equilibrium conversion obtained from the assumption of ideal-gas behavior for the reacting mixture, exhibit significant deviations at low values of the ethylene to water feed mole ratio, with respect to both sets of predictions (molecular simulation and thermodynamic model). The minimum deviation between the ideal gas assumption and the

results from the thermodynamic model is 7.8% at 30 atm, 8.7% at 40 atm, 9.0% at 50 atm, and 9.1% at 60 atm.

By means of the thermodynamic model, in the first of our previous works [1], we calculated the minimum value r_{min} (at the bubble-point) and maximum value r_{max} (at the dew-point) of the ethylene to water feed mole ratio r for the existence of two phases at the chemical equilibrium of the ternary system at 200°C. Those values were reported in Table 12 of Ref. [1]. The ranges $r_{min} < r < r_{max}$ (over which the two-phase system occurs) or $r < r_{min}$ (over which a single liquid phase occurs) can be used to determine whether the conditions chosen to calculate the vapor-phase chemical equilibrium are valid or not. The values of 0.1, 0.3, 0.5, 0.7, 0.8, 0.86, and 0.9 for the initial ethylene mole fraction y_1^0, from which the molecular simulations were started, correspond to r values of 0.1111, 0.4286, 1.0000, 2.3333, 4.0000, 6.1429, and 9.0000, respectively. At 30 atm, the thermodynamic model [1] predicts that the two-phase system occurs for $0.0575 < r < 0.6977$; therefore, the vapor-phase chemical equilibrium compositions shown in Fig. 1 for values of 0.1 and 0.3 for y_1^0 would be hypothetical, because the reaction would actually occur in a two-phase system. At 40 atm, the thermodynamic model predicts that the two-phase system occurs for $0.1262 < r < 1.0030$ and a single liquid phase occurs for $r < 0.1262$; therefore, the vapor-phase chemical equilibrium compositions shown in Fig. 2 for values of 0.1, 0.3, and 0.5 for y_1^0 would also be hypothetical because the reaction would actually occur either in a single liquid phase (for $y_1^0 = 0.1$) or in a two-phase system (for $y_1^0 = 0.3$ and $y_1^0 = 0.5$). At 50 atm, the thermodynamic model predicts that the two-phase system occurs for $0.2393 < r < 1.2358$ and a single liquid phase occurs for $r < 0.2393$; therefore, the vapor-phase chemical equilibrium compositions shown in Fig. 3 for values of 0.1, 0.3, and 0.5 for y_1^0 would also be hypothetical for the same reason given at 40 atm. Finally, at 60 atm, the thermodynamic model predicts that the two-phase system occurs for $0.3734 < r < 1.4279$ and a single liquid phase occurs for $r < 0.3734$; therefore, the vapor-phase chemical equilibrium compositions shown in Fig. 4 for values of 0.1, 0.3, and 0.5 for y_1^0 would also be hypothetical for the same reason given at 40 and 50 atm.

Accordingly, some of the computed values of the vapor-phase equilibrium conversion of ethylene to ethanol shown in Figs. 5-8 would be hypothetical: the ethylene conversions for *r* values of 0.1111 and 0.4286 at 30 atm (Fig. 5), and the ethylene conversions for *r* values of 0.1111, 0.4286, and 1.0000 at 40, 50, and 60 atm (Figs. 6-8).

3.2 Results for the combined chemical and vapor-liquid equilibrium

By following the four-stage strategy explained in Section 2.2, RxGEMC simulations of the combined ChVLE of the ternary system ethylene + water + ethanol were carried out at a temperature of 200°C and at 11 values of pressure. The resulting phase diagrams are shown in Figs. 9-14 (at 30, 40, 50, 60, 80, and 100 atm) and Figs. S1-S5 (at 70, 90, 110, 130, and 150 atm), the latter of which are reported as Supplementary data in Appendix A.

The upper and lower solid curved lines correspond to the dew-point and bubble-point loci of the non-reacting ternary system, respectively. Several tie lines are drawn in each diagram to show the coexisting phases at VLE equilibrium. The dew-point and bubble-point lines as well as the corresponding solid tie lines were calculated by means of the PRSV2-WS-UNIQUAC thermodynamic model as described in detail in the first of our previous works [1]. The dashed tie lines correspond to the molecular simulation results. The filled circles in Figs. 9-14 correspond to simulation results for the coexisting phases of the non-reacting system. The dotted line in the single vapor-phase region of each diagram corresponds to the compositions of the ternary system in vapor-phase chemical equilibrium, as calculated from the thermodynamic model, so that the intersection point of that dotted line with the dew-point line of the non-reacting system corresponds to the vapor phase at the combined ChVLE from the thermodynamic model. In each diagram, the two empty squares correspond to the compositions of the two phases at the combined ChVLE calculated from the thermodynamic model, whereas the two filled squares correspond to the compositions of the two phases at the combined ChVLE computed from molecular simulation.

For most of the pressures listed above, simulation predictions for the composition of the liquid phase at the combined ChVLE (shown by the lower filled squares), turn out to be relatively close

to the corresponding predictions from the thermodynamic model (shown by the lower empty squares); however, at 100 and 130 atm, the deviations between the two sets of predictions become significant. In contrast, for most of the pressure values, simulation predictions for the composition of the vapor phase (shown by the upper filled squares) exhibit significant deviations with respect to the corresponding predictions from the thermodynamic model (shown by the upper empty squares). Both sets of predictions are in relatively close agreement only at 40, 50, and 70 atm.

In Section 3.1, from the predictions that we had previously made by means of the thermodynamic model [1], we tested the validity of the computed values for the vapor-phase chemical equilibrium compositions (shown in Figs. 1-4) and conversions of ethylene to ethanol (shown in Figs. 5-8), arriving at the conclusion that at some conditions of ethylene to water feed mole ratio, the results shown in Figs. 1-8 would be hypothetical because, in accordance with the thermodynamic model, at those conditions, the reaction would actually occur either in a single liquid phase or in a two-phase system. This conclusion turns out to be validated by the fact that the portion of the vapor-phase chemical equilibrium locus that contains the points corresponding to those conditions (see Figs. 1-4) indeed happens to fall inside the two-phase envelope (see Figs. 9-12).

From Figs. 9-14 and S1-S5, it follows that the two phases at the combined ChVLE get richer in ethanol and also their compositions get closer as the pressure increases from 30 to 150 atm. By following the formulation given by Ung and Doherty [46], it is possible to gather the combined ChVLE information given in Figs. 9-14 and S1-S5 in a single reactive phase diagram (valid at 200°C) if ethanol (3) is chosen as the reference component and transformed composition variables are defined for ethylene (1) and water (2), as follows:

$$X_1 = \frac{x_1 + x_3}{1 + x_3} \quad , \quad X_2 = \frac{x_2 + x_3}{1 + x_3} \tag{10-a}$$

$$Y_1 = \frac{y_1 + y_3}{1 + y_3} \quad , \quad Y_2 = \frac{y_2 + y_3}{1 + y_3} \tag{10-b}$$

Each pair of transformed variables sum to unity; therefore, they are not independent and only one variable of each pair is needed to plot the reactive phase diagram. From the results represented by the empty and filled squares in Figs. 9-14 and S1-S5, the reactive phase diagram of pressure versus transformed liquid and vapor-phase ethylene compositions ($P - X_1, Y_1$ diagram) at 200°C was plotted and is shown in Fig. 15, where the filled circles correspond to molecular simulation results and the solid lines correspond to the results obtained by means of the thermodynamic model, which were reported in the first of our previous works [1]. The solid line and filled circles at the left side of the diagram correspond to the reactive bubble-point line, and the solid line and filled circles at the right side of the diagram correspond to the reactive dew-point line. The solid lines intersect at the point marked by the empty circle, at a pressure of 155 atm. As discussed in our previous work [1], since the $P - X_1, Y_1$ plot is touched by a horizontal tangent line at that intersection point, such a point can be regarded as a reactive critical point.

In contrast to the thermodynamic model, molecular simulation predicts a wider reactive phase diagram (due to a reactive dew-point line much richer in ethylene). However, these two independent approaches are in very good agreement with regard to the predicted bubble-point line of the reactive phase diagram. Lines (not shown) passing through the upper simulation data points intersect at a point (indicated by the topmost filled circle) which turns out to be very close to the point marked by the empty circle. Therefore, molecular simulation agrees with the thermodynamic model with regard to the approximate location of the reactive critical point of the ternary system ethylene + water + ethanol.

4. Conclusions

Reaction-ensemble (RxMC) molecular simulation predictions for the vapor-phase chemical equilibrium composition of the ternary system and the equilibrium conversion of ethylene to ethanol (at a temperature of 200°C and pressures of 30, 40, 50, and 60 atm) are in good

agreement with predictions made by use of a thermodynamic model that combines the Peng-Robinson-Stryjek-Vera equation of state, the Wong-Sandler mixing rules, and the UNIQUAC activity coefficient model [1].

The reactive Gibbs-ensemble (RxGEMC) molecular simulation predictions for the bubble-point line of the reactive phase diagram and the approximate location of the reactive critical point are in very good agreement with the predictions made by means of the thermodynamic model. However, due to a reactive dew-point line much richer in ethylene, molecular simulation predicts a wider reactive phase diagram.

Nomenclature

C	number of species in the reacting system
k_B	Boltzmann constant
K_{eq}	chemical equilibrium constant
N	total number of molecules
N_i	initial number of molecules of component *i* for a reaction step
P	pressure
P_{rx}	probability of acceptance of a reaction step
P^0	standard-state pressure
T	absolute temperature
U	configurational energy
V	volume of the simulation box
x_i	liquid-phase mole fraction of component *i*
X_i	transformed liquid-phase mole fraction of component *i*
y_i	vapor-phase mole fraction of component *i*
Y_i	transformed vapor-phase mole fraction of component *i*

Greek symbols

χ	correction factor for the Lorentz-Berthelot combining rule
ν_i	stoichiometric coefficient of component *i*
$\bar{\nu}$	stoichiometric coefficient of the reaction
ζ	reaction direction index

Subscripts

Coul	Coulombic
LJ	Lennard-Jones
t	total

Superscripts

(*b*)	in the backward direction
(*c*)	by creation
(*d*)	by deletion
(*f*)	in the forward direction
real	real-space contribution
recip	reciprocal-space contribution
self	self-interaction contribution

Acknowledgement

Financial support from the Colombian Administrative Department of Science, Innovation and Technology (COLCIENCIAS), through a research assistanship for doctoral students, and additional financial assistance from the Thermodynamics and Energy Technology Chair of the University of Paderborn in Germany during a doctoral-student research internship spent from October 2013 to July 2014, are gratefully acknowledged by one of the authors (Y.M. Muñoz-Muñoz).

References

[1] M. Llano-Restrepo, Y.M. Muñoz-Muñoz, Fluid Phase Equilibr. 307 (2011) 45-57.

[2] Y.M. Muñoz-Muñoz, M. Llano-Restrepo, Fluid Phase Equilibr. 394 (2015) 1-11.

[3] S.L. Weitz, J.J. Potoff, Fluid Phase Equilibr. 234 (2005) 144-150.

[4] Y.-L. Huang, T. Merker, M. Heilig, H. Hasse, J. Vrabec, Ind. Eng. Chem. Res. 51 (2012) 7428-7440.

[5] T. Schnabel, J. Vrabec, H. Hasse, Fluid Phase Equilibr. 233 (2005) 134-143.

[6] J. Smukala, R. Span, W. Wagner, J. Phys. Chem. Ref. Data 29 (2000) 1053-1121.

[7] W. Wagner, A. Pruß, J. Phys. Chem. Ref. Data 31 (2002) 387-535.

[8] H.E. Dillon, S.G. Penoncello, Int. J. Thermophys. 25 (2004) 321-335.

[9] D.S. Tsiklis, E.V. Mushkina, L.I. Shenderei, Inzh. Fiz. Zh. 1 (8) (1958) 3-7.

[10] D.S. Tsiklis, A.N. Kofman, Russ. J. Phys. Chem. 35 (1961) 549-551.

[11] F. Barr-David, B.F. Dodge, J. Chem. Eng. Data 4 (1959) 107-121.

[12] D.S. Tsiklis, A.I. Kulikova, L.I. Shenderei, Khim. Promst. (5) (1960) 401-406.

[13] D.-Y. Peng, D.B. Robinson, Ind. Eng. Chem. Fundam. 15 (1976) 59-64.

[14] R. Stryjek, J.H. Vera, Can. J. Chem. Eng. 64 (1986) 323-333.

[15] D.S.H. Wong, S.I. Sandler, AIChE J. 38 (1992) 671-680.

[16] D.S. Abrams, J.M. Prausnitz, AIChE J. 21 (1975) 116-128.

[17] W.R. Smith, B. Triska, J. Chem. Phys. 100 (1994) 3019-3027.

[18] J.K. Johnson, A.Z. Panagiotopoulos, K.E. Gubbins, Mol. Phys. 81 (1994) 717-733.

[19] C.H. Turner, J.K. Brennan, M. Lísal, W.R. Smith, J.K. Johnson, K.E. Gubbins, Mol. Simul. 34 (2008) 119-146.

[20] C.H. Turner, J.K. Johnson, K.E. Gubbins, J. Chem. Phys. 114 (2001) 1851-1859.

[21] M. Lísal, J.K. Brennan, W.R. Smith, J. Chem. Phys. 124 (2006) 064712.

[22] M. Lísal, P. Cosoli, W.R. Smith, S.K. Jain, K.E. Gubbins, Fluid Phase Equilibr. 272 (2008) 18-31.

[23] C.H. Turner, K.E. Gubbins, J. Chem. Phys. 119 (2003) 6057-6067.

[24] J. Carrero-Mantilla, M. Llano-Restrepo, Fluid Phase Equilibr. 219 (2004) 181-193.

[25] X. Peng, W. Wang, S. Huang, Fluid Phase Equilibr. 231 (2005) 138-149.

[26] M. Lísal, M. Bendová, W.R. Smith, Fluid Phase Equilibr. 235 (2005) 50-57.

[27] J. Carrero-Mantilla, M. Llano-Restrepo, Fluid Phase Equilibr. 242 (2006) 189-203.

[28] M. Lísal, I. Nezbeda, W.R. Smith, J. Chem. Phys. 110 (1999) 8597-8604.

[29] M. Lísal, W.R. Smith, I. Nezbeda, AIChE J. 46 (2000) 866-875.

[30] A.Z. Panagiotopoulos, Mol. Phys. 61 (1987) 813-826.

[31] A.Z. Panagiotopoulos, N. Quirke, M. Stapleton, D.J. Tildesley, Mol. Phys. 63 (1988) 527-545.
[32] A.Z. Panagiotopoulos, M.R. Stapleton, Fluid Phase Equilibr. 53 (1989) 133-141.
[33] A.Z. Panagiotopoulos, Int. J. Thermophys. 10 (1989) 447-457.
[34] B. Smit, Ph. de Smedt, D. Frenkel, Mol. Phys. 68 (1989) 931-950.
[35] B. Smit, D. Frenkel, Mol. Phys. 68 (1989) 951-958.
[36] A.Z. Panagiotopoulos, Mol. Simul. 9 (1992) 1-23.
[37] A.Z. Panagiotopoulos, J. Phys. Condens. Matter 12 (2000) 25-52.
[38] M.P. Allen, D.J. Tildesley, Computer simulation of liquids, Oxford University Press, 1989.
[39] D. Frenkel, B. Smit, Understanding molecular simulation: from algorithms to applications, Second Edition, Academic Press, 2002.
[40] M. Llano-Restrepo, Molecular modeling and Monte Carlo simulation of concentrated aqueous alkali halide solutions at 25°C, Ph.D. Dissertation, Rice University, Houston, 1994.
[41] M. Llano-Restrepo, W.G. Chapman, J. Chem. Phys. 100 (1994) 8321-8339.
[42] D.C. Rapaport, The art of molecular dynamics simulation, Cambridge University Press, 1998.
[43] J.J. de Pablo, J.M. Prausnitz, Fluid Phase Equilibr. 53 (1989) 177-189.
[44] R.P. Fartaria, R.S. Neves, P.C. Rodrigues, F.F. Freitas, F. Silva-Fernandes, Comp. Phys. Comm. 175 (2006) 116-121.
[45] H. Flyvbjerg, H.G. Petersen, J. Chem. Phys. 91 (1989) 461-466.
[46] S. Ung, M.F. Doherty, Chem. Eng. Sci. 50 (1995) 23-48.

VITAE

Y. Mauricio Muñoz-Muñoz received his undergraduate degree (B.S) in chemical engineering from Universidad Nacional de Colombia, at the Manizales campus, in 2007, and his doctoral degree (in Chemical Engineering) from Universidad del Valle, Cali, Colombia, in November 2014. He is currently working as a postdoctoral researcher in the Thermodynamics and Energy Technology Chair of Professor Jadran Vrabec at the Faculty of Mechanical Engineering of the University of Paderborn in Germany.

Jadran Vrabec is Professor of Thermodynamics and Energy Technology at the University of Paderborn, Germany. He received his Ph.D. degree in Mechanical Engineering from Ruhr-

Universität-Bochum in 1996. His main research interests are molecular modeling and simulation, applied experimental thermodynamics, and energy technology. In 2013, he was awarded with the International Supercomputing Award. Some of the courses he has taught are thermodynamics, molecular thermodynamics, rational energy use, and process engineering.

Mario Llano-Restrepo is Professor of Chemical Engineering at Universidad del Valle in Cali, Colombia. He received his Ph.D. degree (in Chemical Engineering) from Rice University in 1994. His main research interests are modeling of phase and chemical equilibria, modeling and simulation of separation processes, and molecular simulation. In 2009, he earned a Distinguished Professor recognition from Universidad del Valle for service and excellence in teaching since 1994. Some of the courses he has taught are chemical thermodynamics, statistical thermodynamics, molecular simulation, chemical reaction engineering, mass transfer, separation operations, and separation process modeling and simulation.

Figure Captions

Figure 1. Vapor-phase chemical equilibrium composition diagram of ethylene + water + ethanol at 200°C and 30 atm. Filled circles: molecular simulation results of this work; empty circles and solid curved line: calculated with the PRSV2-WS-UNIQUAC thermodynamic model; empty squares: feed compositions. Dotted lines join feed (initial) and equilibrium (final) compositions.

Figure 2. Vapor-phase chemical equilibrium composition diagram of ethylene + water + ethanol at 200°C and 40 atm. Filled circles: molecular simulation results of this work; empty circles and solid curved line: calculated with the PRSV2-WS-UNIQUAC thermodynamic model; empty squares: feed compositions. Dotted lines join feed (initial) and equilibrium (final) compositions.

Figure 3. Vapor-phase chemical equilibrium composition diagram of ethylene + water + ethanol at 200°C and 50 atm. Filled circles: molecular simulation results of this work; empty circles and solid curved line: calculated with the PRSV2-WS-UNIQUAC thermodynamic model; empty squares: feed compositions. Dotted lines join feed (initial) and equilibrium (final) compositions.

Figure 4. Vapor-phase chemical equilibrium composition diagram of ethylene + water + ethanol at 200°C and 60 atm. Filled circles: molecular simulation results of this work; empty circles and solid curved line: calculated with the PRSV2-WS-UNIQUAC thermodynamic model; empty squares: feed compositions. Dotted lines join feed (initial) and equilibrium (final) compositions.

Figure 5. Vapor-phase reaction equilibrium percentage conversion of ethylene to ethanol at 200°C and 30 atm as a function of the ethylene to water feed mole ratio. Filled circles: molecular simulation results of this work; solid curved line calculated with the PRSV2-WS-UNIQUAC thermodynamic model; empty squares: calculated by assuming ideal-gas behavior.

Figure 6. Vapor-phase reaction equilibrium percentage conversion of ethylene to ethanol at 200°C and 40 atm as a function of the ethylene to water feed mole ratio. Filled circles: molecular simulation results of this work; solid curved line calculated with the PRSV2-WS-UNIQUAC thermodynamic model; empty squares: calculated by assuming ideal-gas behavior.

Figure 7. Vapor-phase reaction equilibrium percentage conversion of ethylene to ethanol at 200°C and 50 atm as a function of the ethylene to water feed mole ratio. Filled circles: molecular simulation results of this work; solid curved line calculated with the PRSV2-WS-UNIQUAC thermodynamic model; empty squares: calculated by assuming ideal-gas behavior.

Figure 8. Vapor-phase reaction equilibrium percentage conversion of ethylene to ethanol at 200°C and 60 atm as a function of the ethylene to water feed mole ratio. Filled circles: molecular

simulation results of this work; solid curved line calculated with the PRSV2-WS-UNIQUAC thermodynamic model; empty squares: calculated by assuming ideal-gas behavior.

Figure 9. Combined ChVLE phase diagram of ethylene + water + ethanol at 200°C and 30 atm. Filled squares joined by a dashed line: ChVLE molecular simulation results of this work; empty squares joined by a solid line: ChVLE results obtained with the PRSV2-WS-UNIQUAC thermodynamic model; dotted curved line: vapor-phase chemical equilibrium composition locus; upper solid curved line: non-reactive dew-point locus; lower solid curved line: non-reactive bubble-point locus; filled circles joined by dashed lines: non-reactive VLE molecular simulation results; solid line segments: non-reactive VLE tie lines calculated with the thermodynamic model.

Figure 10. Combined ChVLE phase diagram of ethylene + water + ethanol at 200°C and 40 atm. Filled squares joined by a dashed line: ChVLE molecular simulation results of this work; empty squares joined by a solid line: ChVLE results obtained with the PRSV2-WS-UNIQUAC thermodynamic model; dotted curved line: vapor-phase chemical equilibrium composition locus; upper solid curved line: non-reactive dew-point locus; lower solid curved line: non-reactive bubble-point locus; filled circles joined by dashed lines: non-reactive VLE molecular simulation results; solid line segments: non-reactive VLE tie lines calculated with the thermodynamic model.

Figure 11. Combined ChVLE phase diagram of ethylene + water + ethanol at 200°C and 50 atm. Filled squares joined by a dashed line: ChVLE molecular simulation results of this work; empty squares joined by a solid line: ChVLE results obtained with the PRSV2-WS-UNIQUAC thermodynamic model; dotted curved line: vapor-phase chemical equilibrium composition locus; upper solid curved line: non-reactive dew-point locus; lower solid curved line: non-reactive bubble-point locus; filled circles joined by dashed lines: non-reactive VLE molecular simulation

results; solid line segments: non-reactive VLE tie lines calculated with the thermodynamic model.

Figure 12. Combined ChVLE phase diagram of ethylene + water + ethanol at 200°C and 60 atm. Filled squares joined by a dashed line: ChVLE molecular simulation results of this work; empty squares joined by a solid line: ChVLE results obtained with the PRSV2-WS-UNIQUAC thermodynamic model; dotted curved line: vapor-phase chemical equilibrium composition locus; upper solid curved line: non-reactive dew-point locus; lower solid curved line: non-reactive bubble-point locus; filled circles joined by dashed lines: non-reactive VLE molecular simulation results; solid line segments: non-reactive VLE tie lines calculated with the thermodynamic model.

Figure 13. Combined ChVLE phase diagram of ethylene + water + ethanol at 200°C and 80 atm. Filled squares joined by a dashed line: ChVLE molecular simulation results of this work; empty squares joined by a solid line: ChVLE results obtained with the PRSV2-WS-UNIQUAC thermodynamic model; dotted curved line: vapor-phase chemical equilibrium composition locus; upper solid curved line: non-reactive dew-point locus; lower solid curved line: non-reactive bubble-point locus; filled circles joined by dashed lines: non-reactive VLE molecular simulation results; solid line segments: non-reactive VLE tie lines calculated with the thermodynamic model.

Figure 14. Combined ChVLE phase diagram of ethylene + water + ethanol at 200°C and 100 atm. Filled squares joined by a dashed line: ChVLE molecular simulation results of this work; empty squares joined by a solid line: ChVLE results obtained with the PRSV2-WS-UNIQUAC thermodynamic model; dotted curved line: vapor-phase chemical equilibrium composition locus; upper solid curved line: non-reactive dew-point locus; lower solid curved line: non-reactive bubble-point locus; filled circles joined by dashed lines: non-reactive VLE molecular simulation

results; solid line segments: non-reactive VLE tie lines calculated with the thermodynamic model.

Figure 15. Reactive phase diagram (pressure versus transformed liquid and vapor-phase ethylene mole fractions) for the ternary system ethylene + water + ethanol at 200°C. Filled circles: molecular simulation results of this work; solid lines: calculated with the PRSV2-WS-UNIQUAC thermodynamic model; empty circle: reactive critical point predicted by thermodynamic model; topmost filled circle: reactive critical point predicted by molecular simulation.

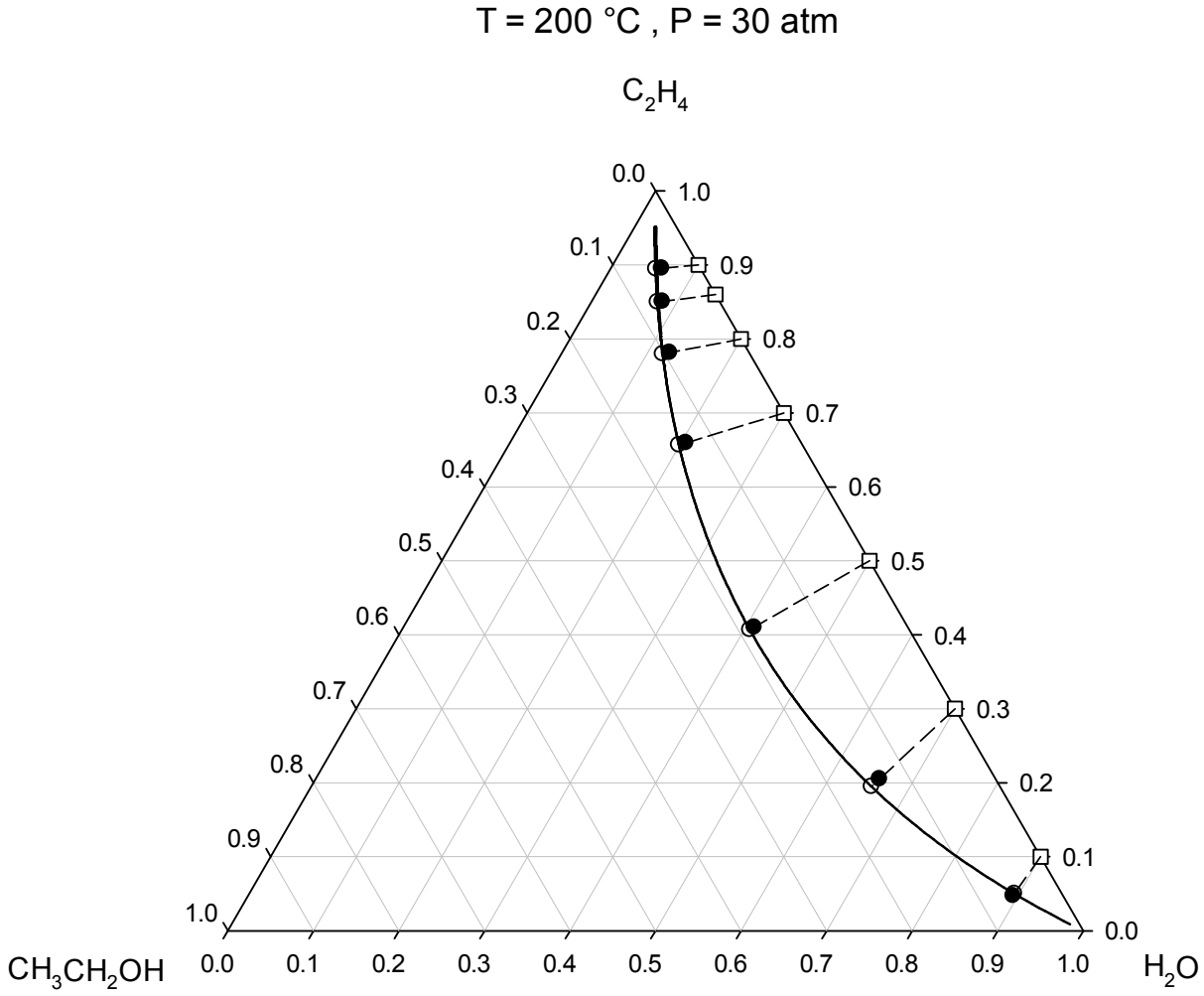

Figure 1

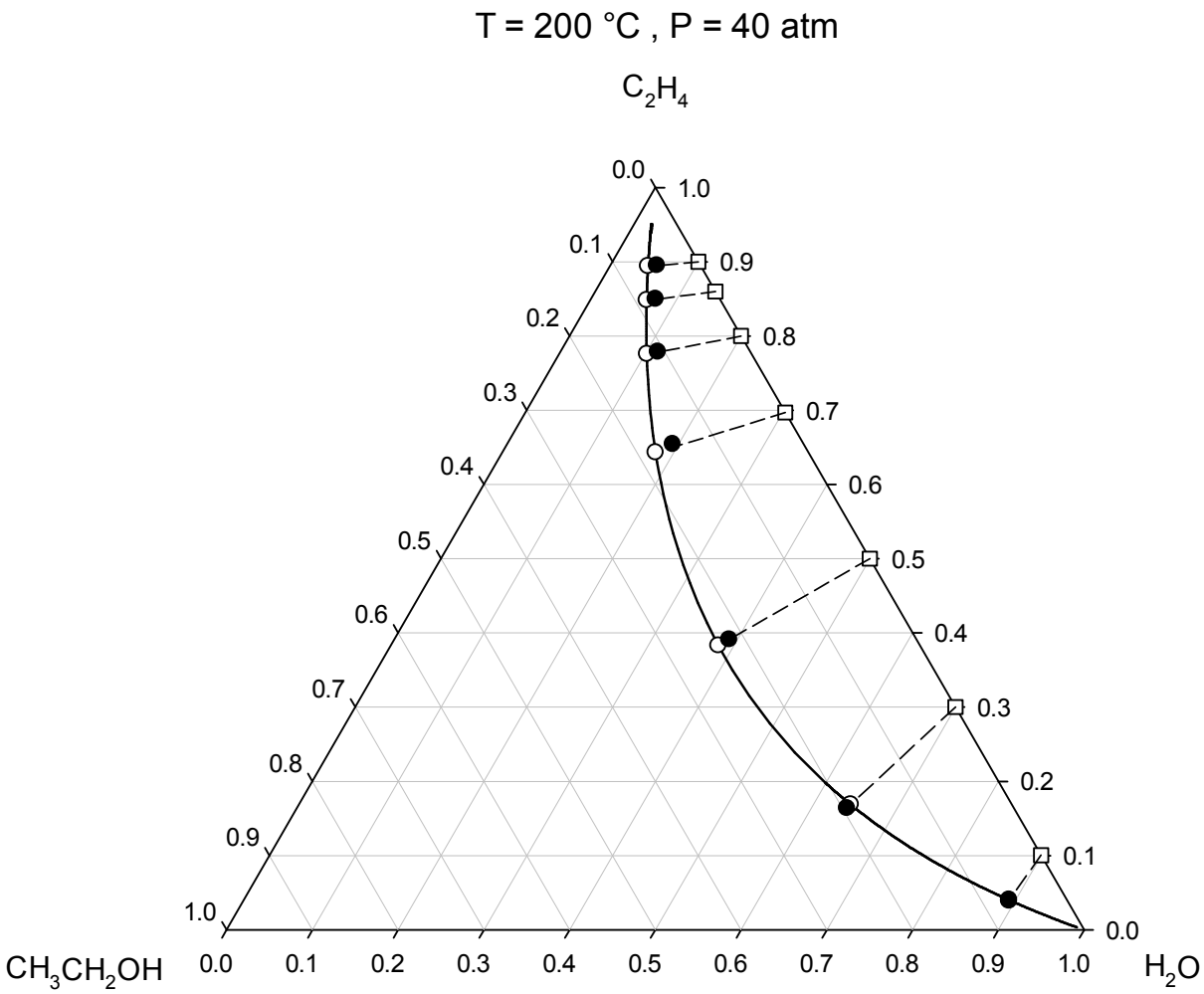

Figure 2

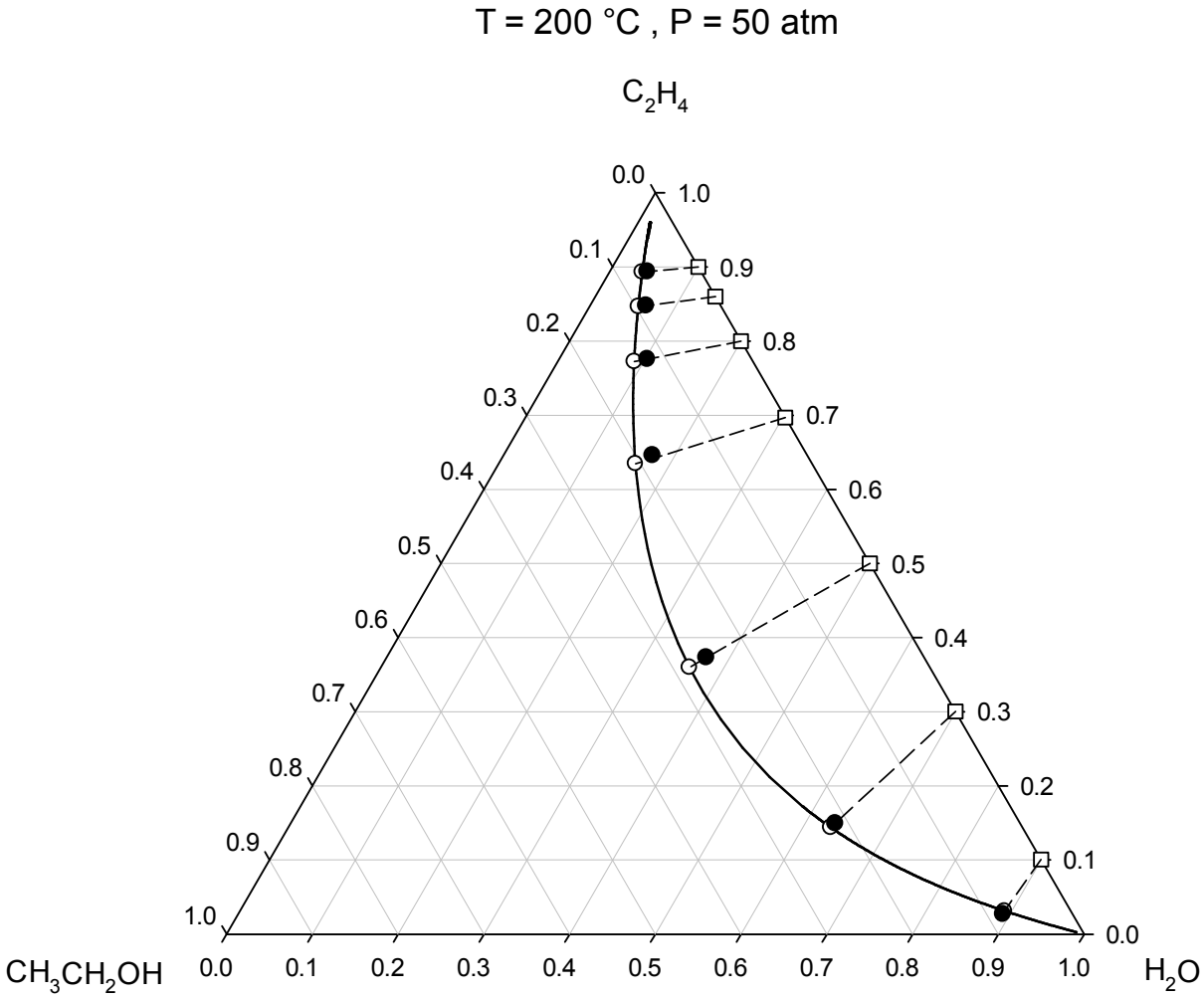

Figure 3

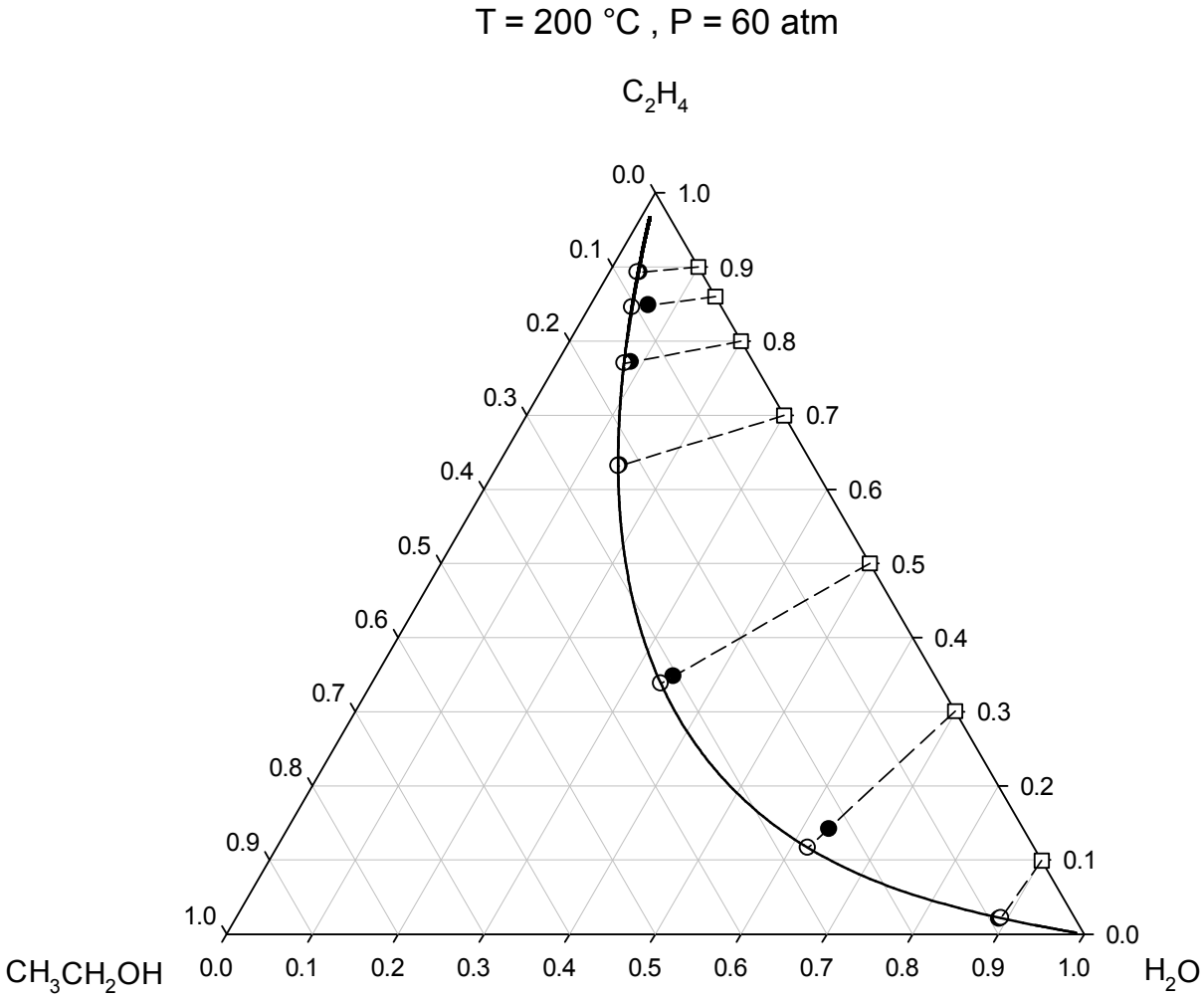

Figure 4

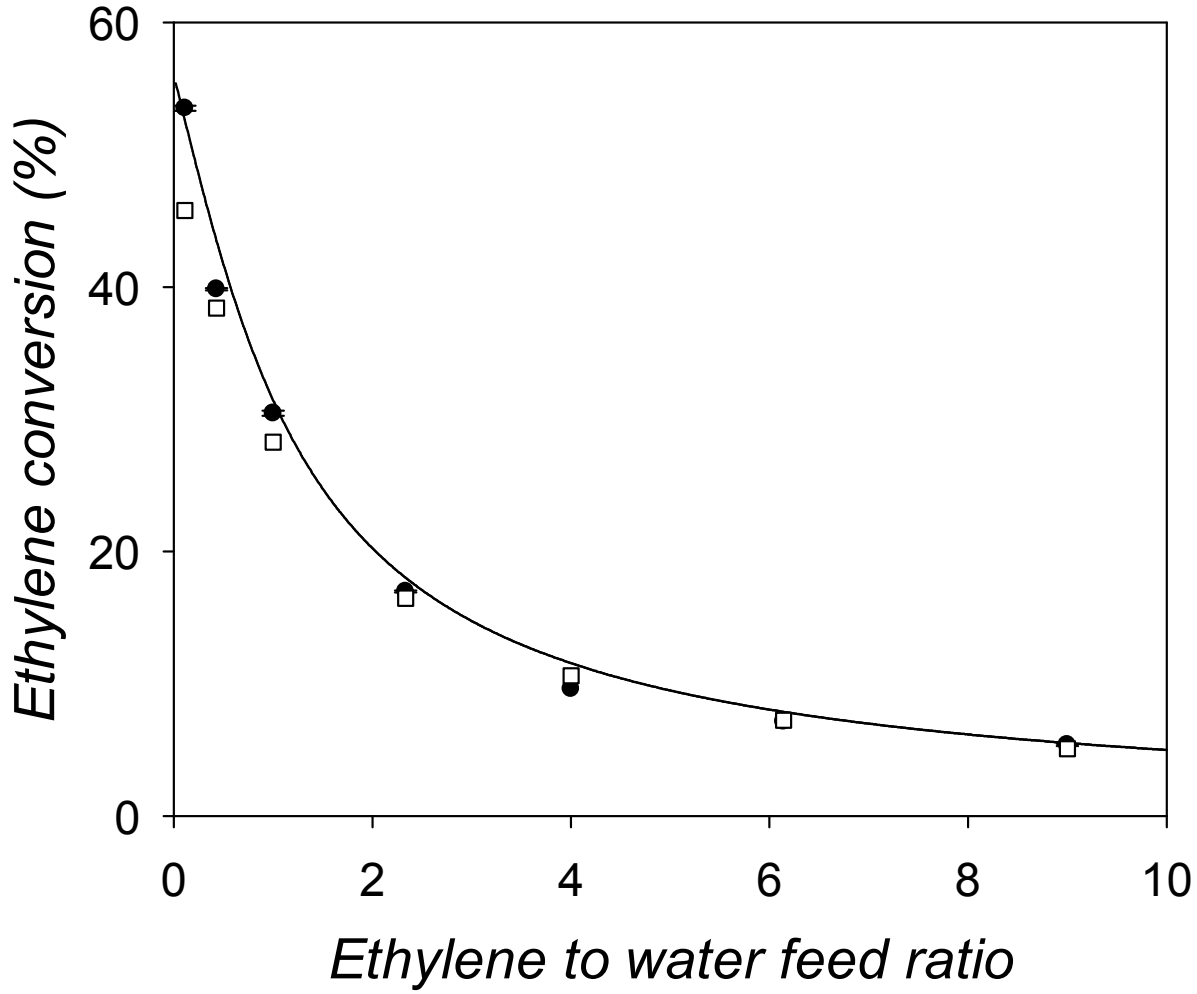
60
40
20
0
Ethylene conversion (%)
0
2
4
6
8
10
Ethylene to water feed ratio

Figure 5

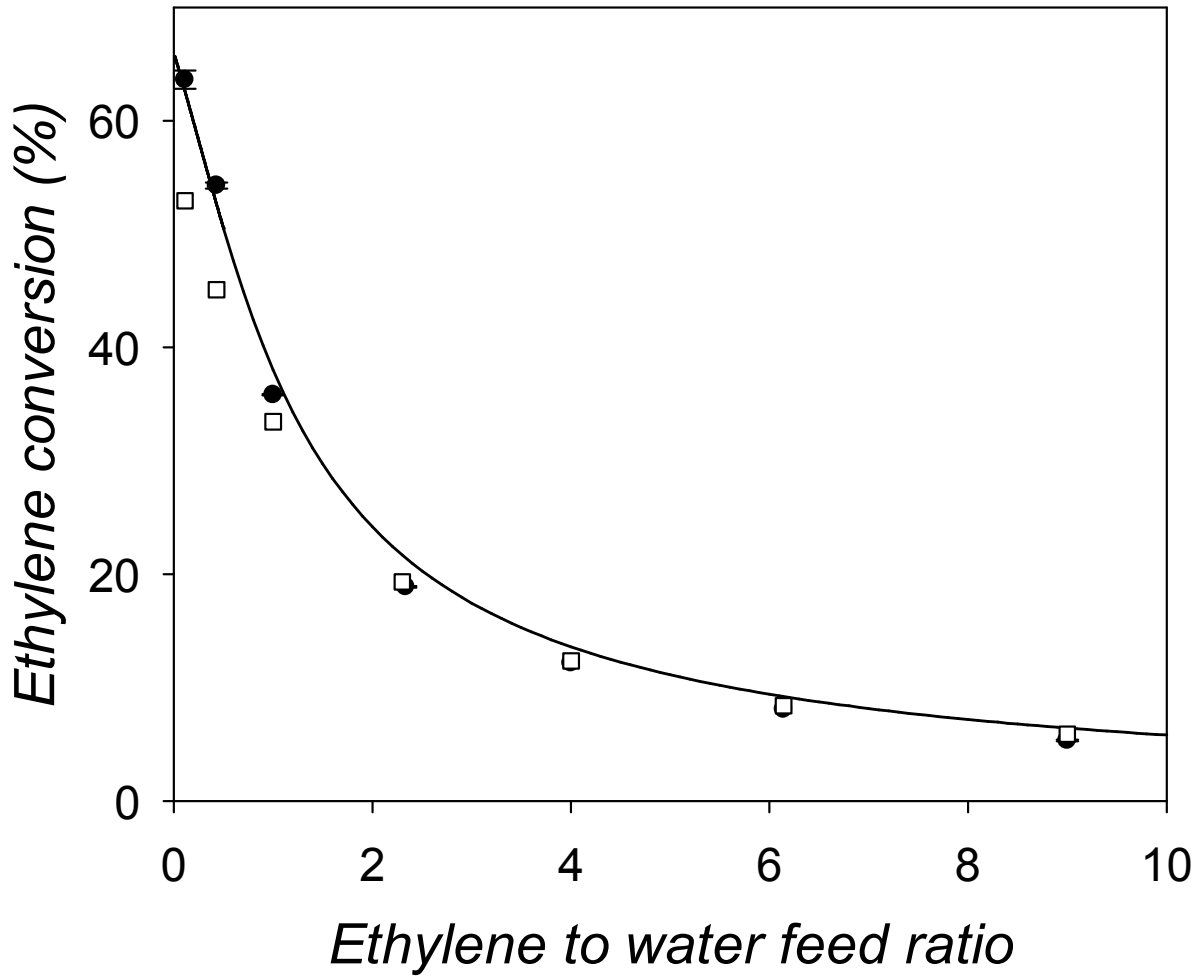
Ethylene conversion (%)
0
20
40
60
0
2
4
6
8
10
Ethylene to water feed ratio

Figure 6

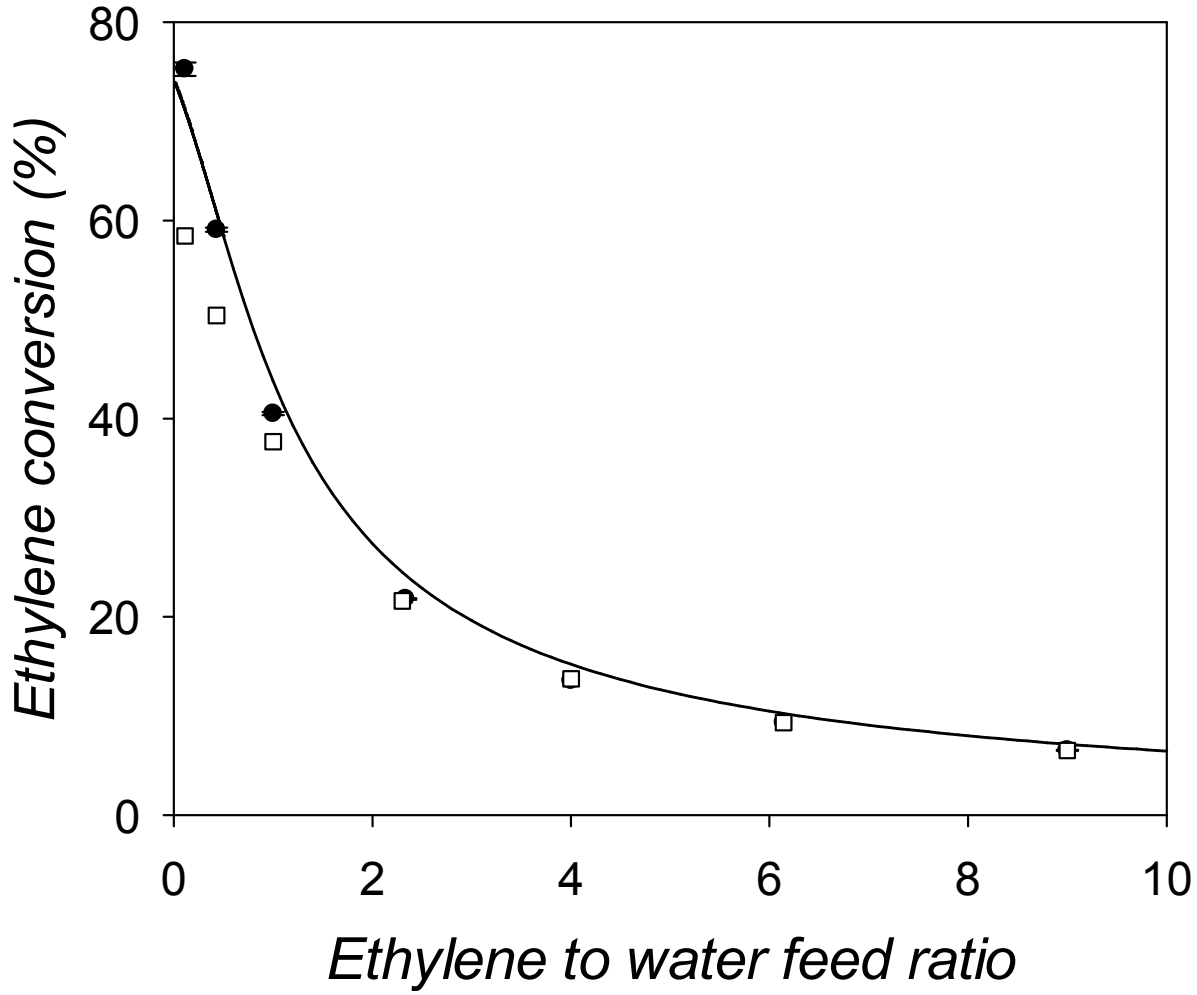
80
60
40
20
0
Ethylene conversion (%)
0
2
4
6
8
10
Ethylene to water feed ratio

Figure 7

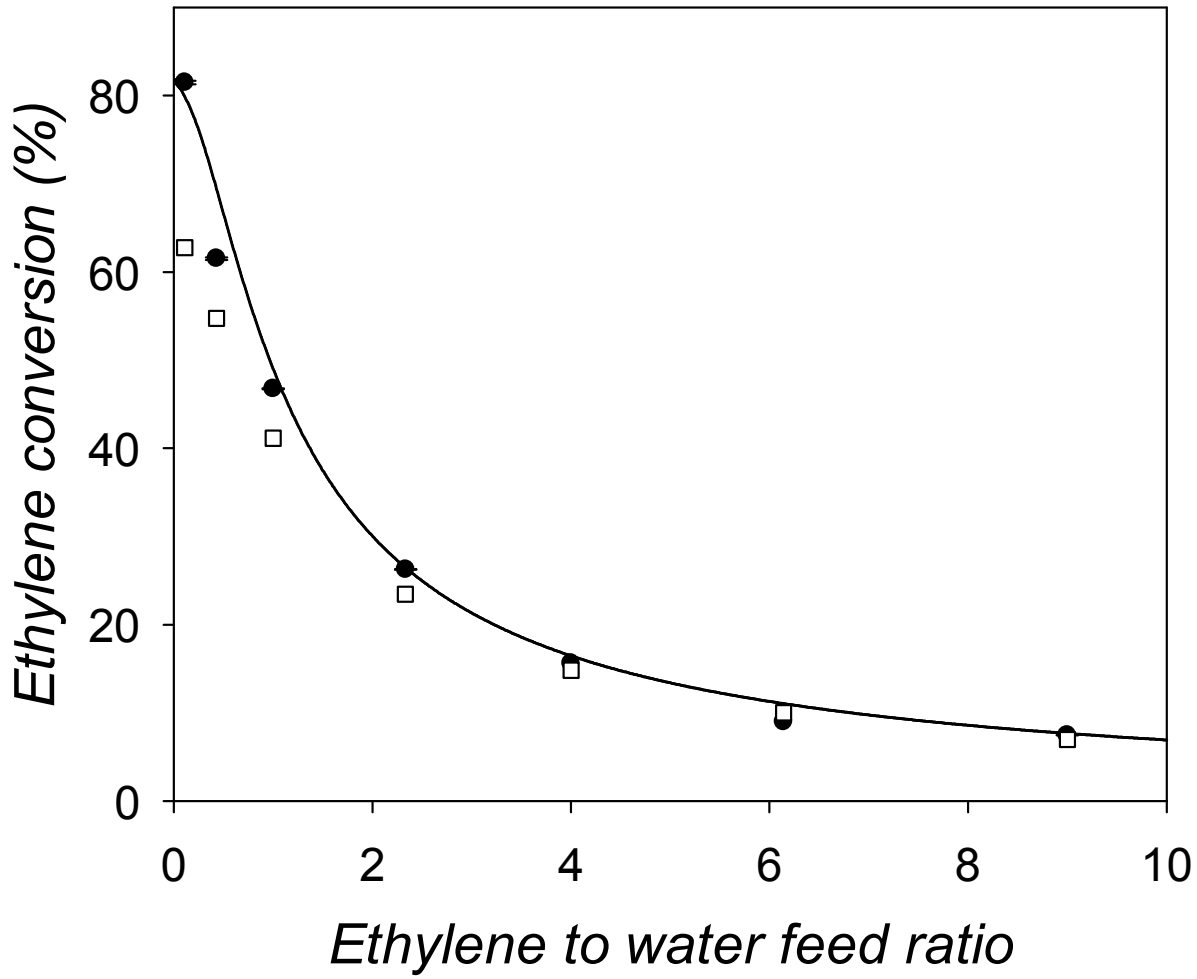
Ethylene conversion (%)
80
60
40
20
0
0
2
4
6
8
10
Ethylene to water feed ratio

Figure 8

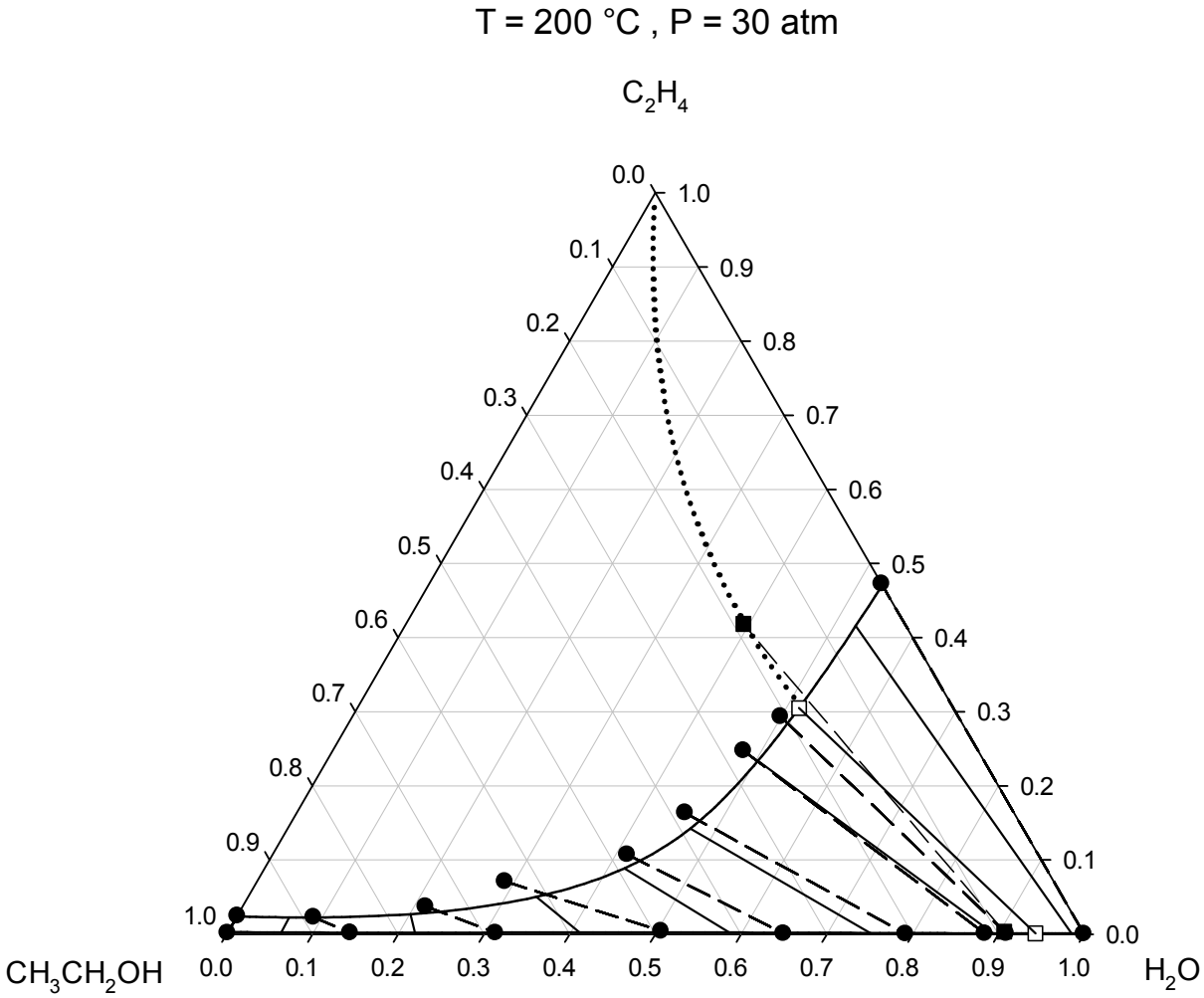

Figure 9

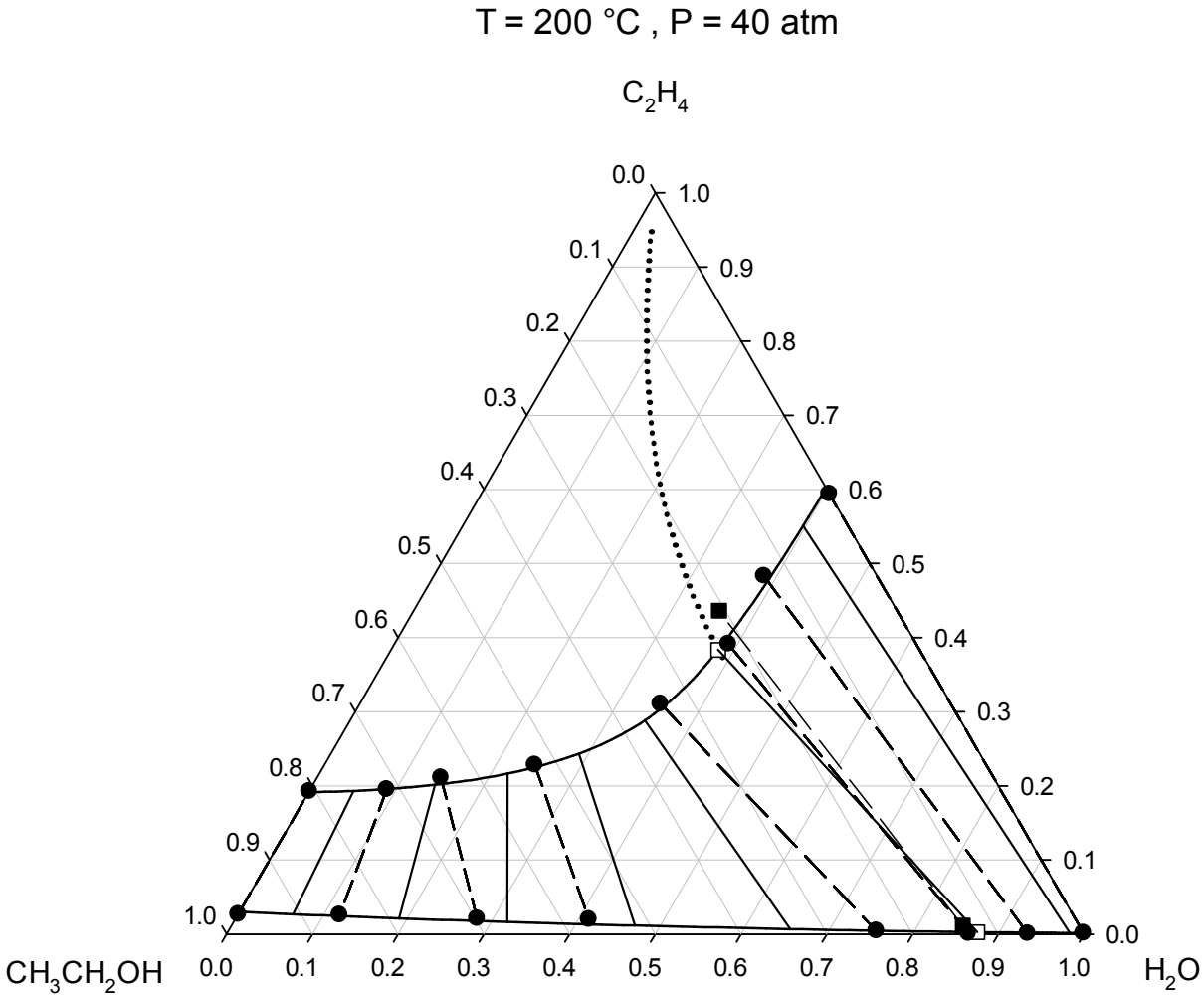

Figure 10

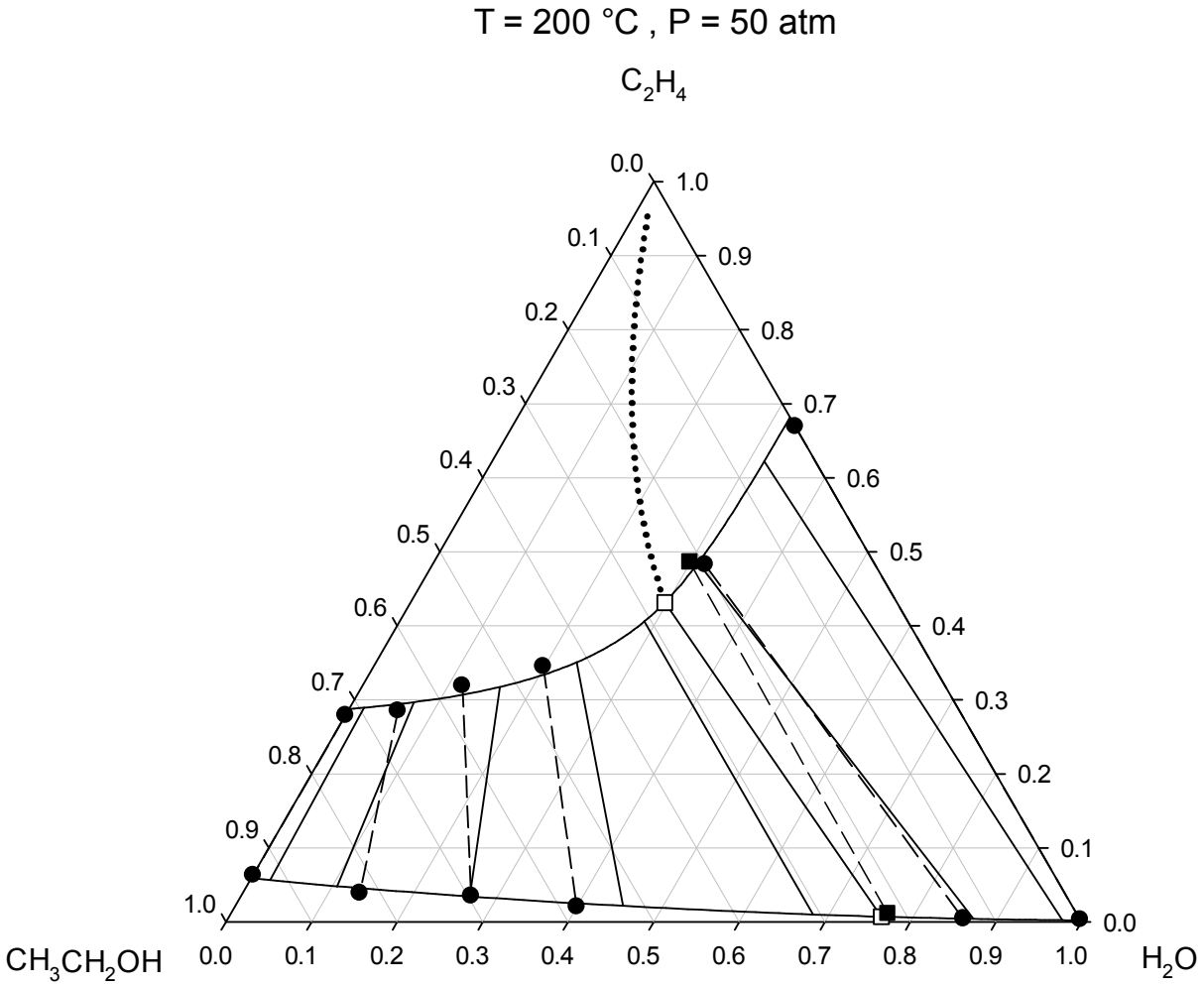

Figure 11

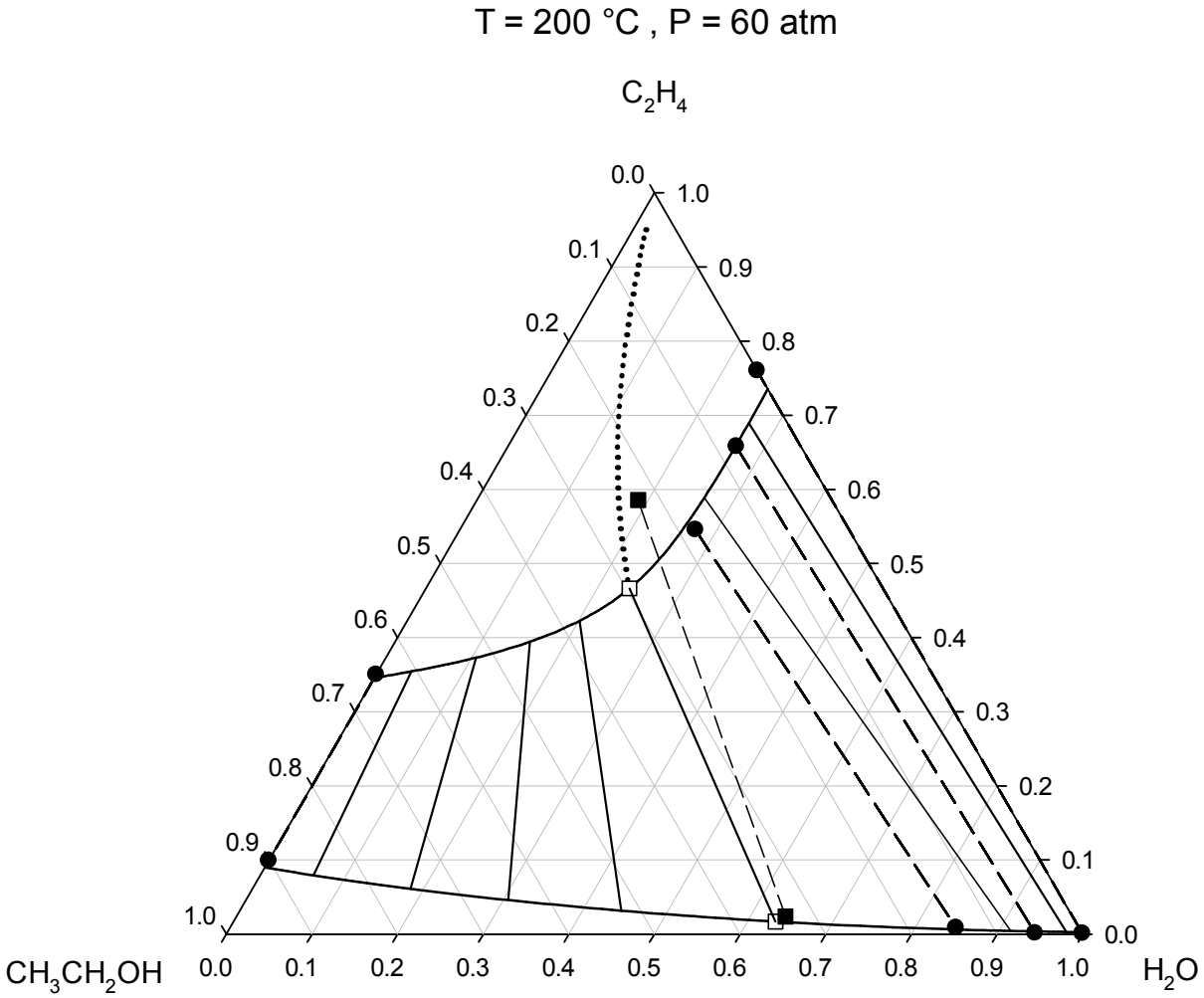

Figure 12

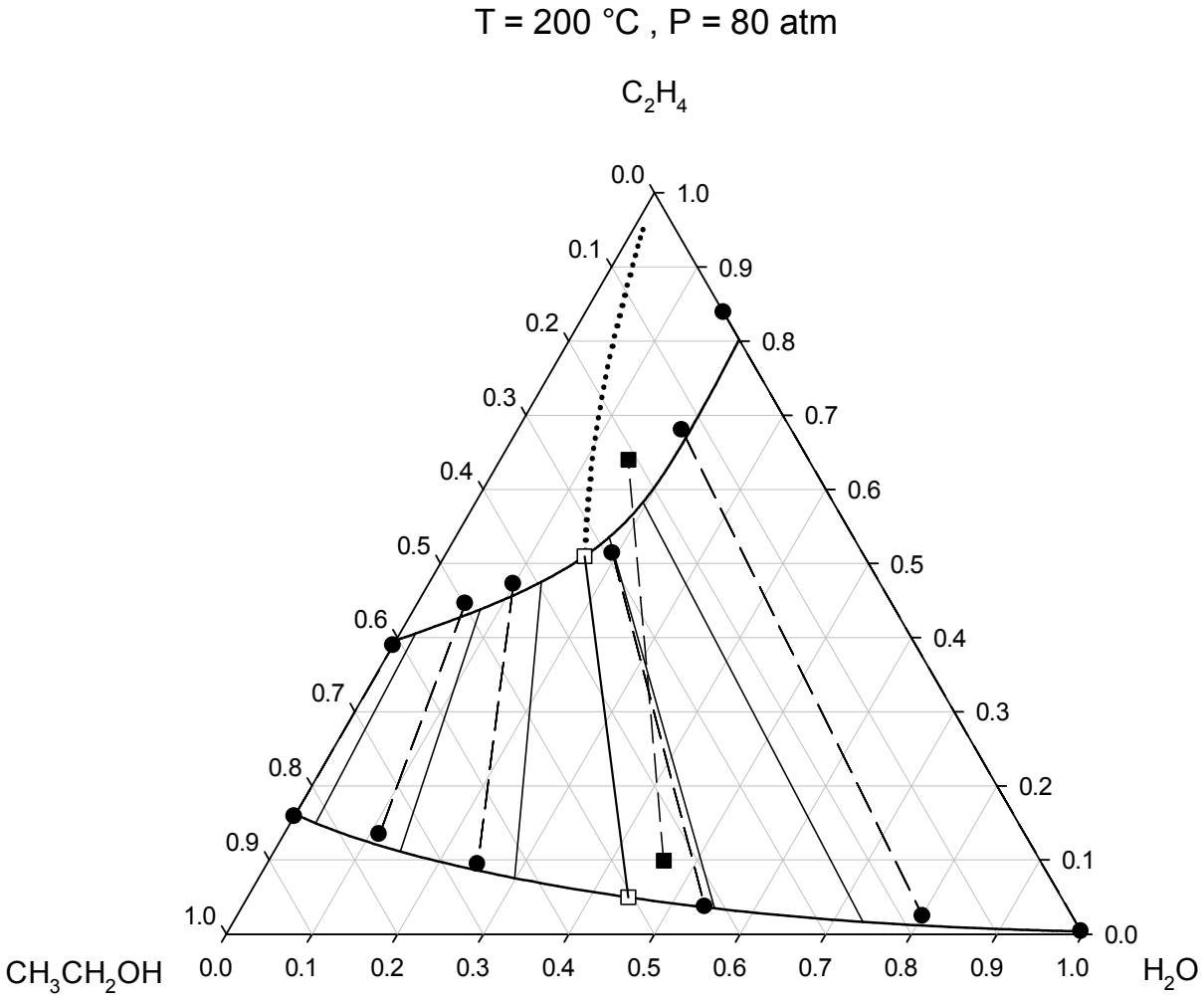

Figure 13

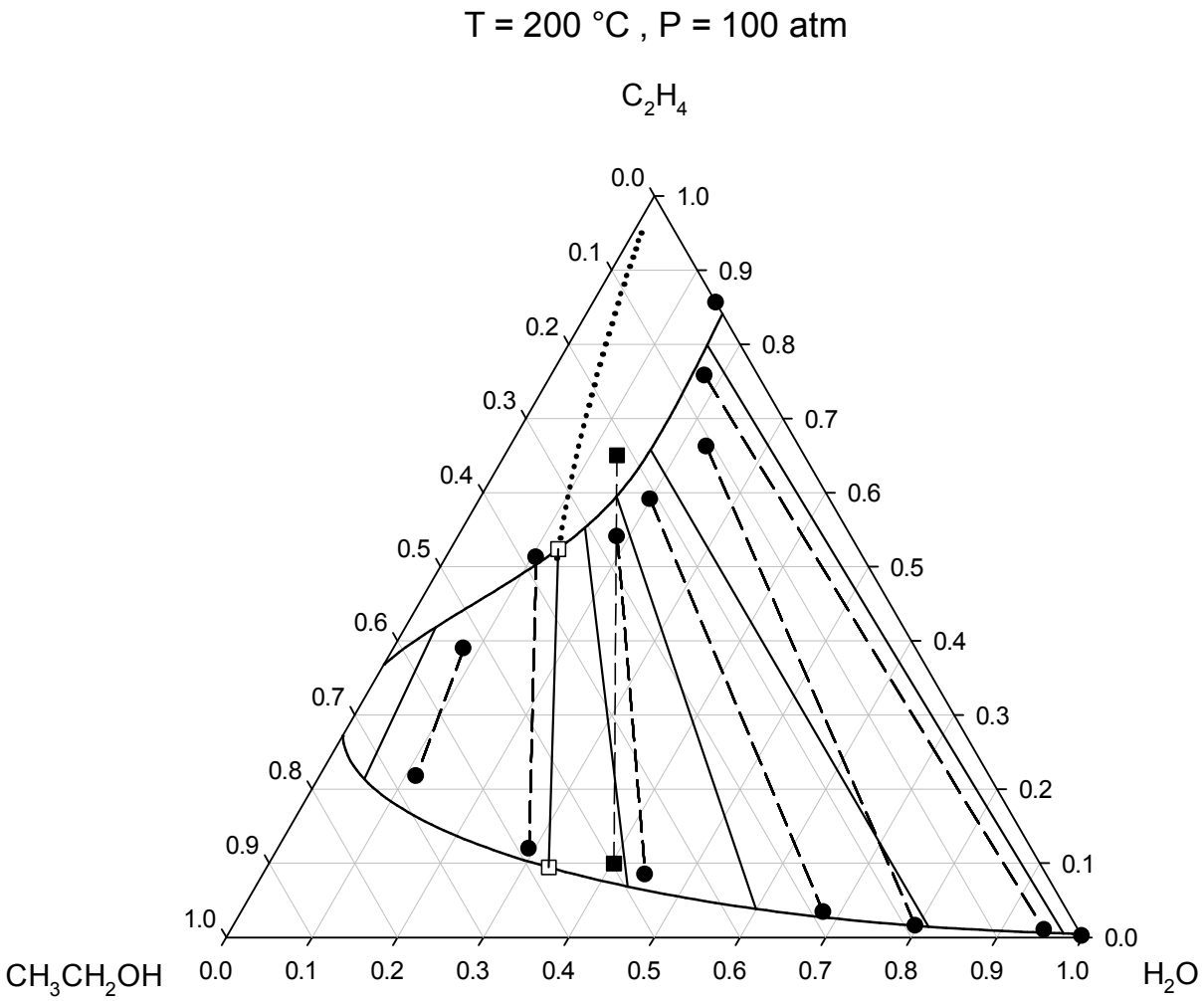

Figure 14

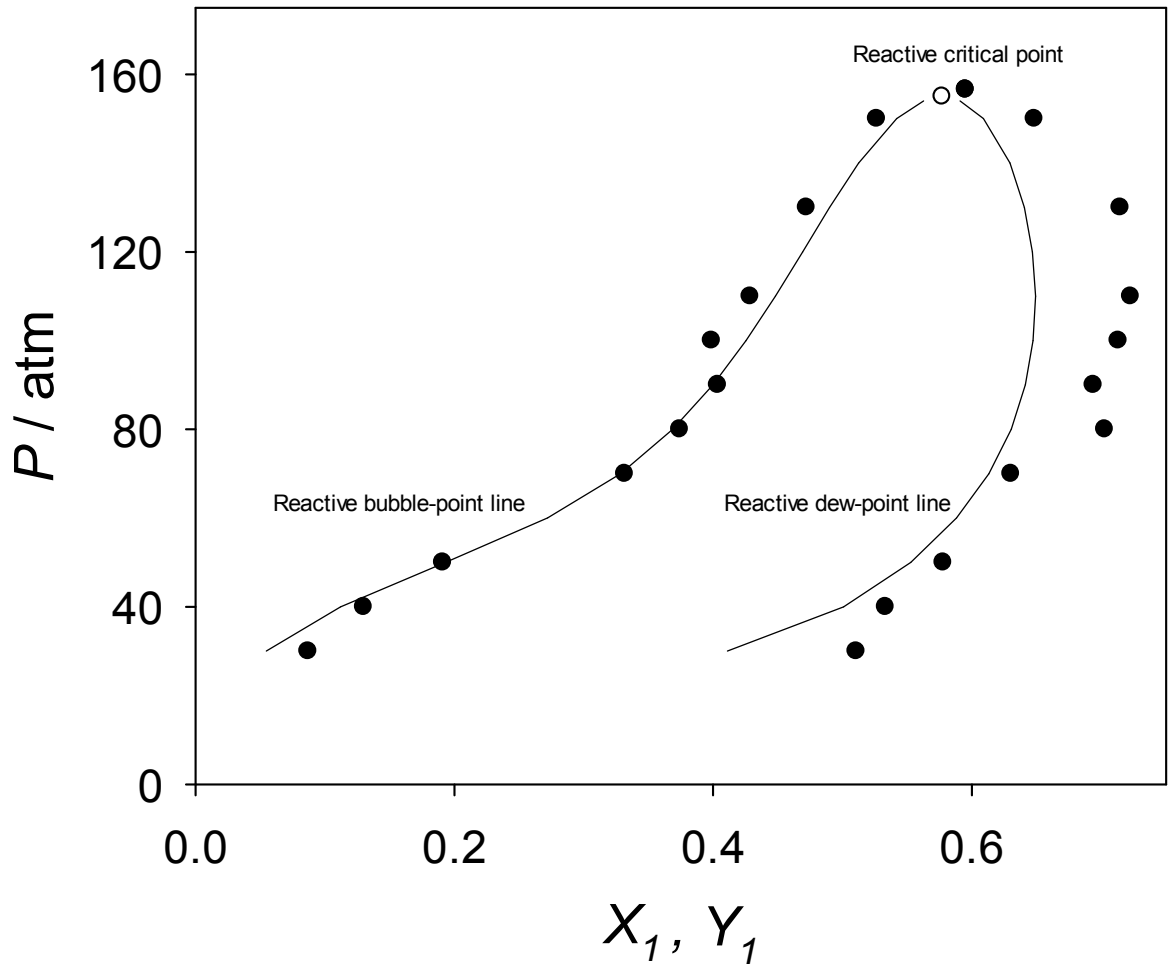
Reactive critical point
Reactive bubble-point line
Reactive dew-point line
160
120
80
40
0
0.0
0.2
0.4
0.6
P / atm
X1, Y1

Figure 15

Supplementary Data for

Vapor-phase chemical equilibrium and combined chemical and vapor-liquid equilibrium for the ternary system ethylene + water + ethanol from reaction-ensemble and reactive Gibbs-ensemble molecular simulations

Y. Mauricio Muñoz-Muñoz [a,b], Jadran Vrabec[b], Mario Llano-Restrepo [a]*

[a] School of Chemical Engineering, Universidad del Valle,
Ciudad Universitaria Melendez, Building 336,
Apartado 25360, Cali, Colombia

[b] Thermodynamics and Energy Technology,
University of Paderborn, 33098 Paderborn, Germany

* Corresponding author. Tel: + 57-2-3312935; fax: + 57-2-3392335
E-mail address: mario.llano@correounivalle.edu.co (M. Llano-Restrepo)

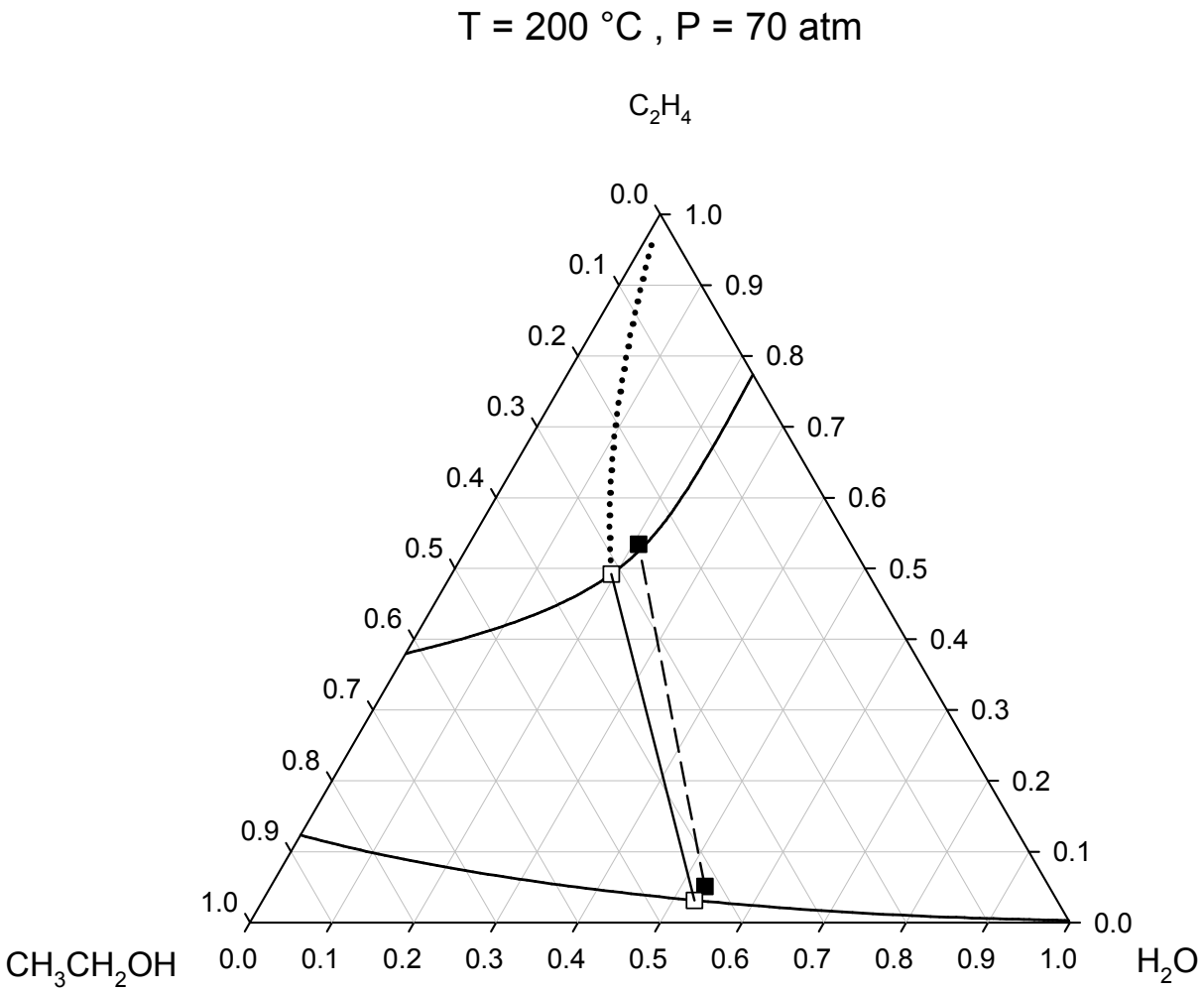

Figure S1. Combined ChVLE phase diagram of ethylene + water + ethanol at 200°C and 70 atm. Filled squares joined by a dashed line: ChVLE molecular simulation results of this work; empty squares joined by a solid line: ChVLE results obtained with the PRSV2-WS-UNIQUAC thermodynamic model; dotted curved line: vapor-phase chemical equilibrium composition locus; upper solid curved line: non-reactive dew-point locus; lower solid curved line: non-reactive bubble-point locus; solid curves calculated with the thermodynamic model.

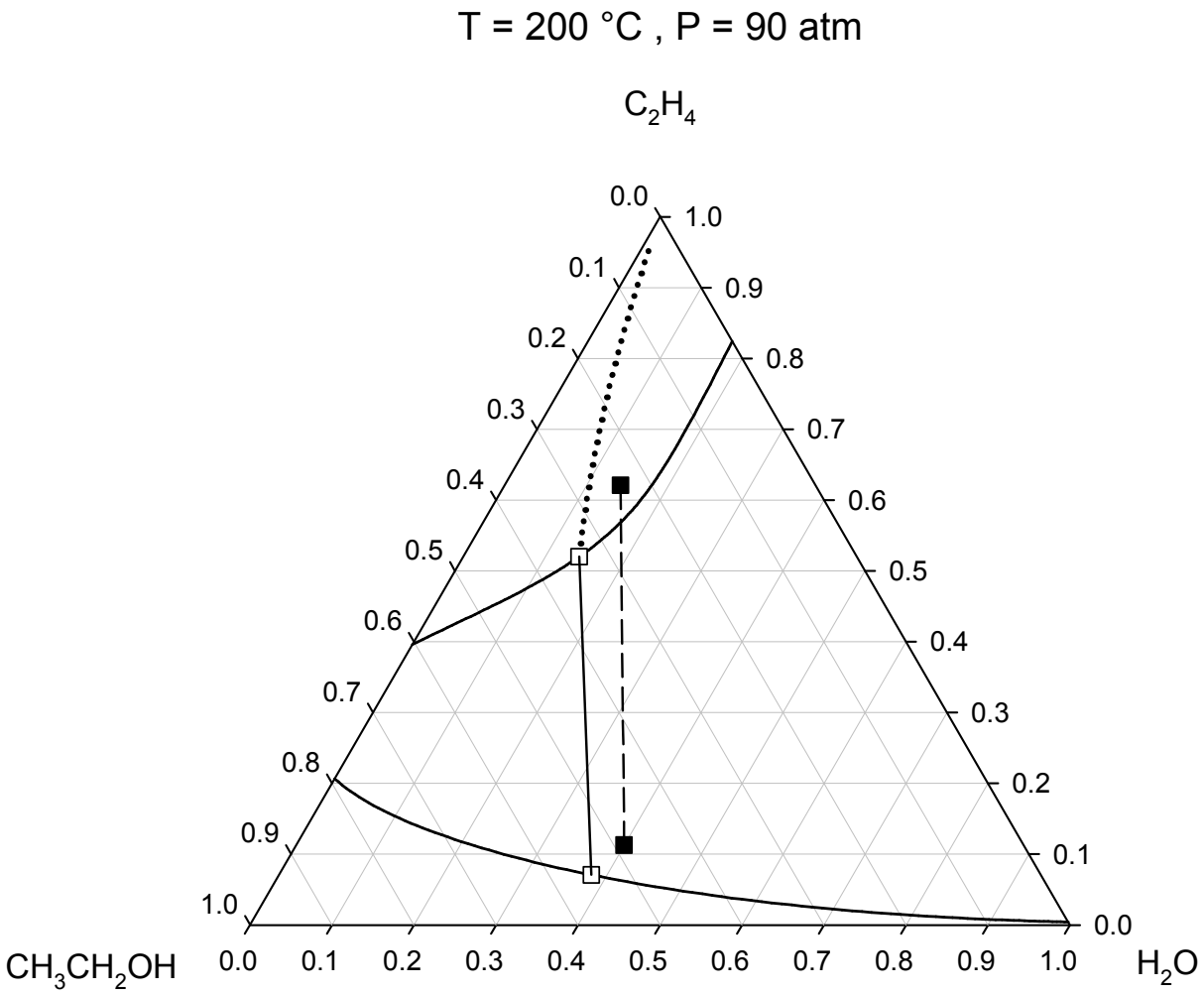

Figure S2. Combined ChVLE phase diagram of ethylene + water + ethanol at 200°C and 90 atm. Filled squares joined by a dashed line: ChVLE molecular simulation results of this work; empty squares joined by a solid line: ChVLE results obtained with the PRSV2-WS-UNIQUAC thermodynamic model; dotted curved line: vapor-phase chemical equilibrium composition locus; upper solid curved line: non-reactive dew-point locus; lower solid curved line: non-reactive bubble-point locus; solid curves calculated with the thermodynamic model.

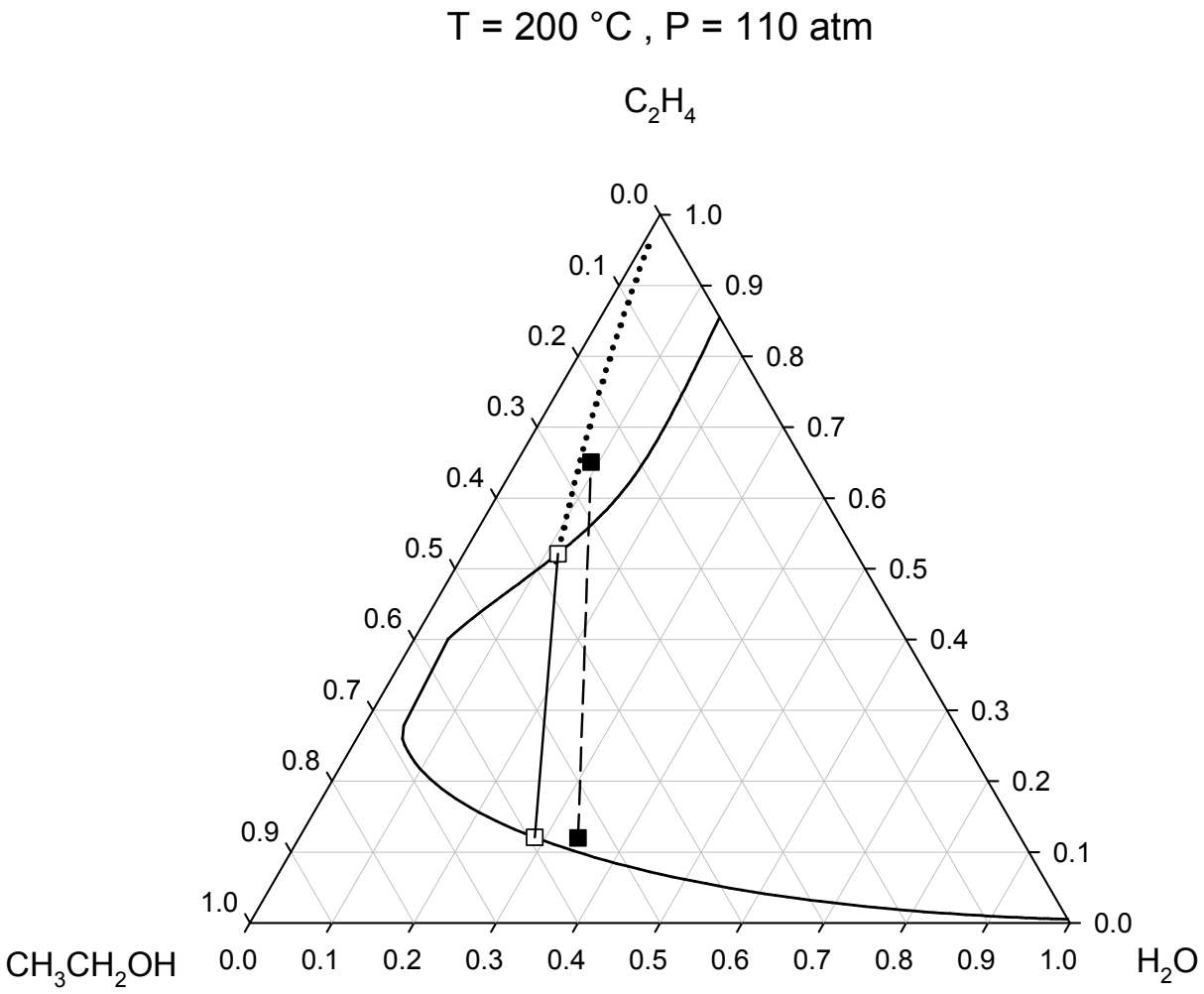

Figure S3. Combined ChVLE phase diagram of ethylene + water + ethanol at 200°C and 110 atm. Filled squares joined by a dashed line: ChVLE molecular simulation results of this work; empty squares joined by a solid line: ChVLE results obtained with the PRSV2-WS-UNIQUAC thermodynamic model; dotted curved line: vapor-phase chemical equilibrium composition locus; upper solid curved line: non-reactive dew-point locus; lower solid curved line: non-reactive bubble-point locus; solid curves calculated with the thermodynamic model.

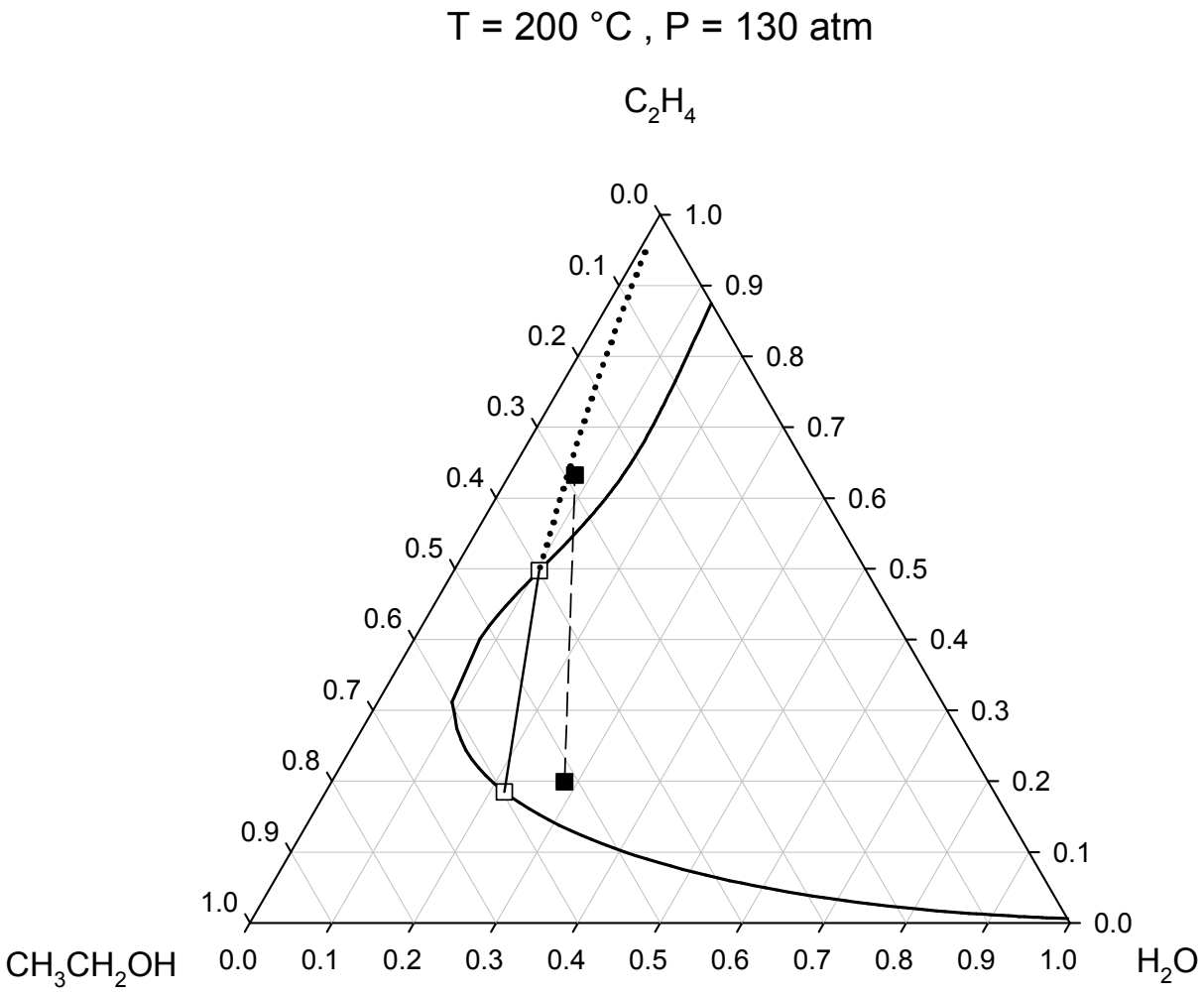

Figure S4. Combined ChVLE phase diagram of ethylene + water + ethanol at 200°C and 130 atm. Filled squares joined by a dashed line: ChVLE molecular simulation results of this work; empty squares joined by a solid line: ChVLE results obtained with the PRSV2-WS-UNIQUAC thermodynamic model; dotted curved line: vapor-phase chemical equilibrium composition locus; upper solid curved line: non-reactive dew-point locus; lower solid curved line: non-reactive bubble-point locus; solid curves calculated with the thermodynamic model.

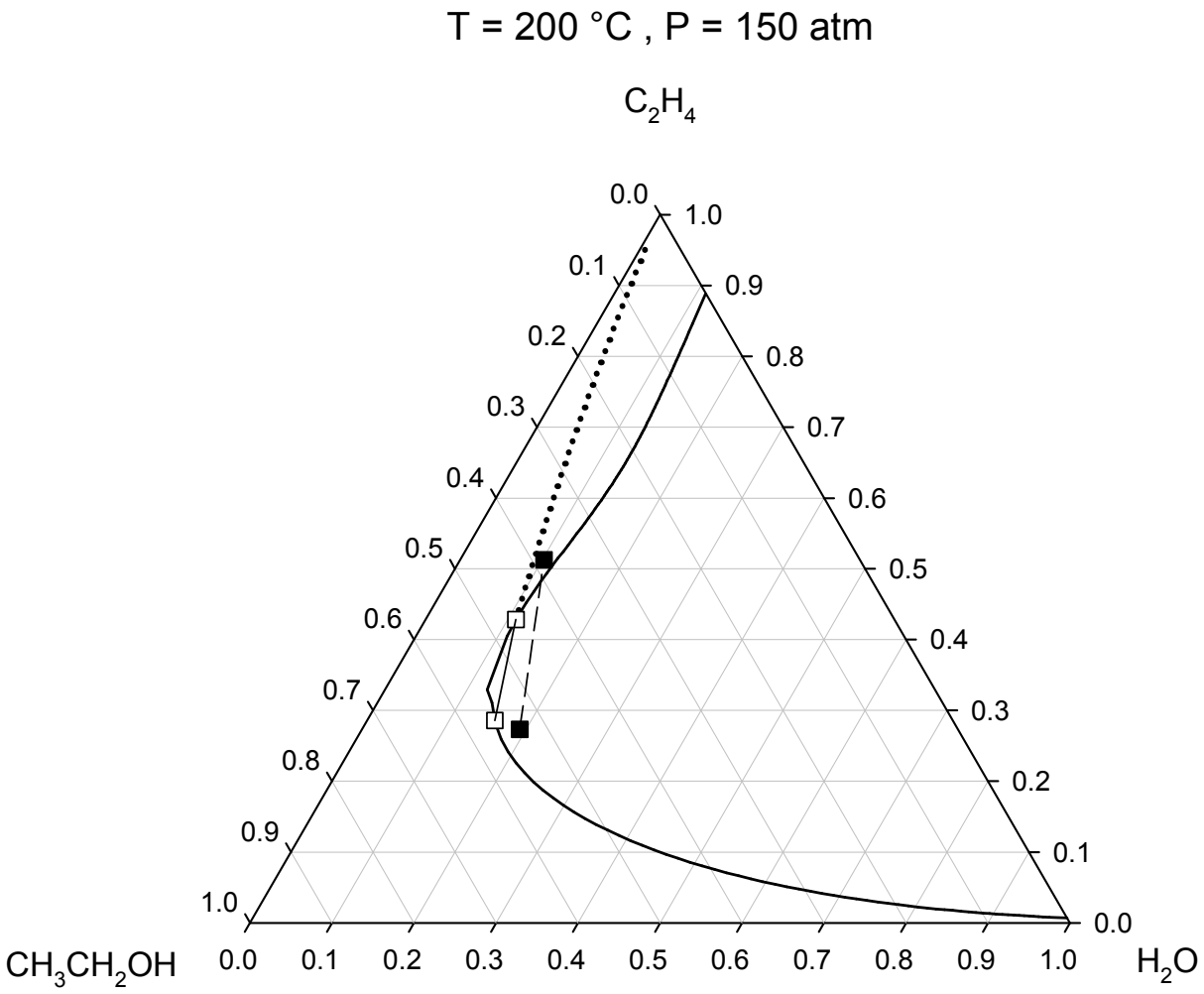

Figure S5. Combined ChVLE phase diagram of ethylene + water + ethanol at 200°C and 150 atm. Filled squares joined by a dashed line: ChVLE molecular simulation results of this work; empty squares joined by a solid line: ChVLE results obtained with the PRSV2-WS-UNIQUAC thermodynamic model; dotted curved line: vapor-phase chemical equilibrium composition locus; upper solid curved line: non-reactive dew-point locus; lower solid curved line: non-reactive bubble-point locus; solid curves calculated with the thermodynamic model.